Article

Neuron

# Spatial and Temporal Organization of the Individual Human Cerebellum

## Graphical Abstract

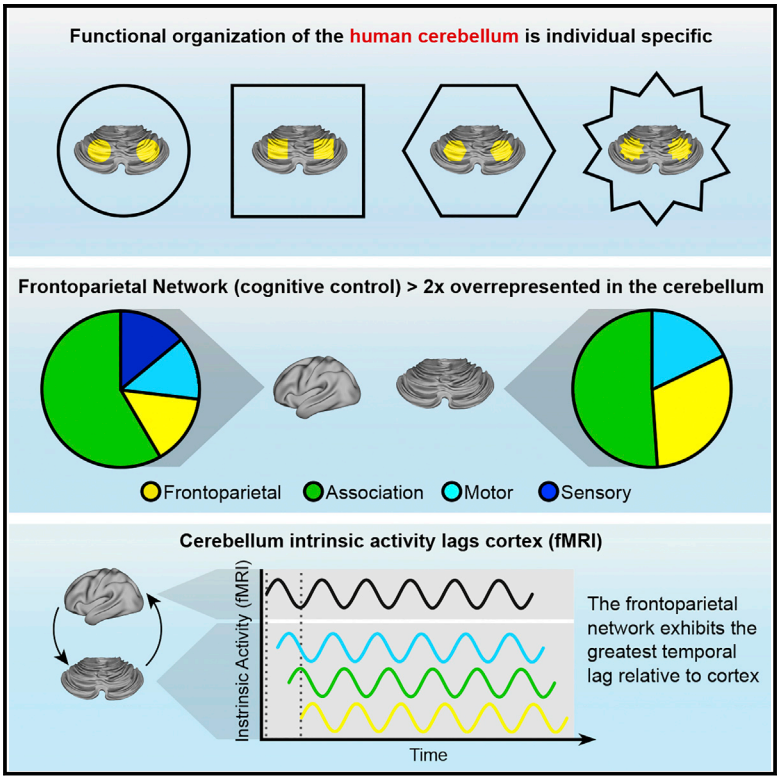


## Authors

Scott Marek, Joshua S. Siegel, Evan M. Gordon, ..., Steven E. Petersen, Deanna J. Greene, Nico U.F. Dosenbach

## Correspondence

smarek@wustl.edu

## In Brief

Cerebellar functional networks are topographically individual-specific. Cerebellar intrinsic fMRI signals lag those in cortex by 100–400 ms. The frontoparietal control network is greatly overrepresented (>2-fold), suggesting that the cerebellum is important for the adaptive control of the brain's cognitive processes.

## Highlights

- Individual-specific functional brain networks can be elucidated in the cerebellum
- Inter-individual variance in cerebellar functional networks exceeds that of cortex
- The frontoparietal control network is 2-fold overrepresented in the cerebellum
- Cerebellar BOLD signals temporally lag the cortex by hundreds of milliseconds

Marek et al., 2018, Neuron *100*, 977–993
November 21, 2018 
https://doi.org/10.1016/j.neuron.2018.10.010

CellPress

Neuron
Article

# Spatial and Temporal Organization of the Individual Human Cerebellum

Scott Marek,[1,15,*] Joshua S. Siegel,[1] Evan M. Gordon,[2,7,8] Ryan V. Raut,[5] Caterina Gratton,[1] Dillan J. Newbold,[1] Mario Ortega,[1] Timothy O. Laumann,[1] Babatunde Adeyemo,[1] Derek B. Miller,[1] Annie Zheng,[1] Katherine C. Lopez,[3] Jeffrey J. Berg,[6] Rebecca S. Coalson,[1,5] Annie L. Nguyen,[1] Donna Dierker,[5] Andrew N. Van,[1] Catherine R. Hoyt,[4] Kathleen B. McDermott,[3,5] Scott A. Norris,[1] Joshua S. Shimony,[5] Abraham Z. Snyder,[1,5] Steven M. Nelson,[2,7,8] Deanna M. Barch,[3,5,9] Bradley L. Schlaggar,[1,5,9,10,11] Marcus E. Raichle,[1,5,12] Steven E. Petersen,[1,3,5,11,12,13] Deanna J. Greene,[5,9,14] and Nico U.F. Dosenbach[1,4,5,10,12,14]
[1]Department of Neurology, Washington University School of Medicine, St. Louis, MO 63110, USA
[2]VISN17 Center of Excellence for Research on Returning War Veterans, Waco, TX 76711, USA
[3]Department of Psychological and Brain Sciences, Washington University in St. Louis, St. Louis, MO 63110, USA
[4]Program in Occupational Therapy, Washington University School of Medicine, St. Louis, MO 63110, USA
[5]Mallinckrodt Institute of Radiology, Washington University School of Medicine, St. Louis, MO 63110, USA
[6]Department of Psychology, New York University, New York, NY 10003 USA
[7]Center for Vital Longevity, School of Behavioral and Brain Sciences, University of Texas at Dallas, Dallas, TX 75235, USA
[8]Department of Psychology and Neuroscience, Baylor University, Waco, TX 76706, USA
[9]Department of Psychiatry, Washington University School of Medicine, St. Louis, MO 63110, USA
[10]Department of Pediatrics, Washington University School of Medicine, St. Louis, MO 63110, USA
[11]Department of Neuroscience, Washington University School of Medicine, St. Louis, MO 63110, USA
[12]Department of Biomedical Engineering, Washington University in St. Louis, St. Louis, MO 63110, USA
[13]Department of Neurological Surgery, Washington University School of Medicine, St. Louis, MO 63110, USA
[14]Senior author
[15]Lead Contact
*Correspondence: smarek@wustl.edu
https://doi.org/10.1016/j.neuron.2018.10.010

## SUMMARY

**The cerebellum contains the majority of neurons in the human brain and is unique for its uniform cytoarchitecture, absence of aerobic glycolysis, and role in adaptive plasticity. Despite anatomical and physiological differences between the cerebellum and cerebral cortex, group-average functional connectivity studies have identified networks related to specific functions in both structures. Recently, precision functional mapping of individuals revealed that functional networks in the cerebral cortex exhibit measurable individual specificity. Using the highly sampled Midnight Scan Club (MSC) dataset, we found the cerebellum contains reliable, individual-specific network organization that is significantly more variable than the cerebral cortex. The frontoparietal network, thought to support adaptive control, was the only network overrepresented in the cerebellum compared to the cerebral cortex (2.3-fold). Temporally, all cerebellar resting state signals lagged behind the cerebral cortex (125–380 ms), supporting the hypothesis that the cerebellum engages in a domain-general function in the adaptive control of all cortical processes.**

## INTRODUCTION

The human cerebellum contains nearly four times as many neurons as the cerebral cortex (hereafter referred to as cortex for brevity) (Andersen et al., 1992) and is markedly different from the cortex in numerous ways, including a high tonic firing rate of principle output neurons (Manns et al., 2004), lack of aerobic glycolysis (Vaishnavi et al., 2010), and greater rate of evolutionary expansion relative to the cortex (3-to 4-fold; Barton and Venditti, 2014). The lateral and posterior portions of the human cerebellum are disproportionately expanded in humans compared to apes and co-activate with cortex across a vast array of control-related functions supported by the frontoparietal network (Marek and Dosenbach, 2018), including error processing (Dosenbach et al., 2006; Fiez, 1996; Fiez et al., 1992), task switching (Monsell, 2003), and language processing (Petersen et al., 1989). Seminal transneuronal tracing studies have shown that the lateral posterior regions of the cerebellum form closed-looped circuits with regions of the premotor, prefrontal, and posterior parietal cortex in macaques (Dum and Strick, 2003; Kelly and Strick, 2003; Strick et al., 2009), providing an anatomical framework for a putative role in adaptive feedback mechanisms for behavioral modification of movement and cognitive processes. Thus, the characterization of the cerebellum purely as a conserved motor structure is antiquated and inaccurate (Buckner, 2013; Caligiore et al., 2017; Fiez, 1996; Leiner et al., 1989; Schmahmann, 2004; Schmahmann et al., 2009; Strick et al., 2009).

Although previous studies have provided an anatomical and functional framework for understanding cerebellar contributions to brain function, the degree of individual specificity in cerebellar functional organization is currently unknown. Quantification of individual cerebellar variability may deepen our understanding of how individual variability in cerebellar functional organization contributes to individual differences in behavior, psychopathology, and clinical outcomes. One promising approach for studying individual cerebellar network organization is through resting state functional connectivity MRI (RSFC), which has revolutionized our understanding of cortical network organization (Krienen and Buckner, 2009; Power et al., 2011; Yeo et al., 2011). However, many RSFC studies are cortico-centric, either omitting discussion of the cerebellum or not including the entirety of the cerebellum during data acquisition or analysis. In an influential study, Buckner and colleagues provided the first group-averaged organizational map of cerebellar functional networks (Buckner et al., 2011). One crucial finding from this work was that association networks, including the frontoparietal network, were represented in the lateral cerebellum, supporting previous anatomical tracing studies and group-average task-based human imaging studies showing increased lateral cerebellar blood-oxygen-level-dependent (BOLD) activity during cognitive tasks (Dosenbach et al., 2006, 2007; Fiez, 1996; Fiez et al., 1992). These group-average studies of cerebellar RSFC, however, use limited quantities of data per individual, restricting our understanding of the degree of individual specificity in cerebellar networks. Moreover, relatively low signal-to-noise ratio within the cerebellum compared to the cortex, coupled with the small folia of the cerebellum, heightens the need for high-fidelity data.

Recent work by Gordon and colleagues demonstrated the importance of precision functional mapping in humans (Gordon et al., 2017c). Precision functional mapping refers to the collection of large quantities of RSFC data (hours) within individual human subjects, which improves the signal-to-noise ratio and allows more precise characterization of functional network organization in individuals (Laumann et al., 2015). One critical finding from these studies is that cortical networks show both common organizational principles across individuals and individual-specific features, unresolvable in group-average data (Braga and Buckner, 2017; Gordon et al., 2017a, 2017b, 2017c; Gratton et al., 2018; Laumann et al., 2015). With respect to the cerebellum, degenerative and acute damage tends to result in individual-specific motor and cognitive deficits (Fiez et al., 1992; Schmahmann and Sherman, 1998), suggesting individualized approaches to studying cerebellar organization would improve our understanding of patient populations.

Theoretical accounts of cerebellar function ascribe it a role in adaptive control and experience-driven adaptive plasticity (Caligiore et al., 2017). Adaptive plasticity requires organized, ongoing communication between relevant brain regions. Such bidirectional communication has previously been observed to manifest in distinct frequencies (Mitra et al., 2016; van Kerkoerle et al., 2014). Recently, Mitra and colleagues analyzed temporal lead/lag relationships across inter-regional BOLD signals to demonstrate that infra-slow activity (ISA) propagates through the human brain in a highly reproducible, state-dependent manner, giving rise to familiar RSFC networks (Mitra et al., 2014, 2015). This lag analysis approach revealed directed ISA between the cortex and hippocampus that was directionally opposite of delta band (0.5–4 Hz) propagated activity. The temporal relationship between ISA and delta activity was subsequently found to be widespread across mouse cortex (Mitra et al., 2018). However, the temporal lead-lag relationships within cerebro-cerebellar loops have not been characterized. As such, an examination of group- and individual-level propagation of ISA, as estimated with BOLD, within the cerebro-cerebellar closed-looped circuitry will provide insights into the temporal organization of the activity shared between these structures.

The goal of the present study was to leverage the highly sampled Midnight Scan Club (MSC) dataset to simultaneously characterize (1) individual specificity and variability in cerebellar RSFC and network organization, as well as (2) group- and individual-level principles regarding the spatial organization of functional networks and the temporal propagation of ISA between the cerebellum and cortex. In each case, we benchmark the cerebellum against the cortex, noting differences in individual variability, network organization, and the temporal propagation of BOLD signals.

## RESULTS

### Reliable Cerebellar RSFC Estimation Requires Large Quantities of Data

We determined the reliability of RSFC correlations within the cerebellum by executing iterative split-half reliability analyses similar to Laumann et al. (2015) and Gordon et al. (2017c) (STAR Methods). Generally, cerebellar RSFC requires double the quantity of data of cortical RSFC to achieve the same level of split-half reliability. For example, excellent split-half reliability ($r > 0.90$) in cortical RSFC was achieved with 45 min of motion-censored data (as reported in Gordon et al., 2017c), whereas equivalent excellent reliability ($r > 0.90$) in cerebellar RSFC was achieved with 90 min of motion censored data (Figures S1A–S1C and S1E). We repeated the reliability analysis voxel-wise across the cortex and cerebellum (as opposed to vertices in the cortex) to equate the measurement of two structures and observed this same principle (Figure S1D). Thus, typical RSFC data quantities (i.e., <30 min per individual) are not sufficient to provide stable estimates of individual cerebellar RSFC.

### Individual Cerebellar Networks Share Common Features With—and Deviate from—the Group Average

Previous group-average studies have suggested that some of the cortical functional networks are also represented in the cerebellum (Buckner et al., 2011; O'Reilly et al., 2010). We determined cerebellar functional network organization using a winner-take-all approach (WTA; STAR Methods; Buckner et al., 2011; Choi et al., 2012; Greene et al., 2014; Hwang et al., 2017), assigning each cerebellar voxel to the cortical network to which it displayed the largest average correlation (Figure 1; for flat map WTA representations, see Figure S2; for cortical network assignments, see Figure S3). Several qualitative observations can be made in the group average (Figure 1A). Supporting previous results, foot, hand, and face motor representations

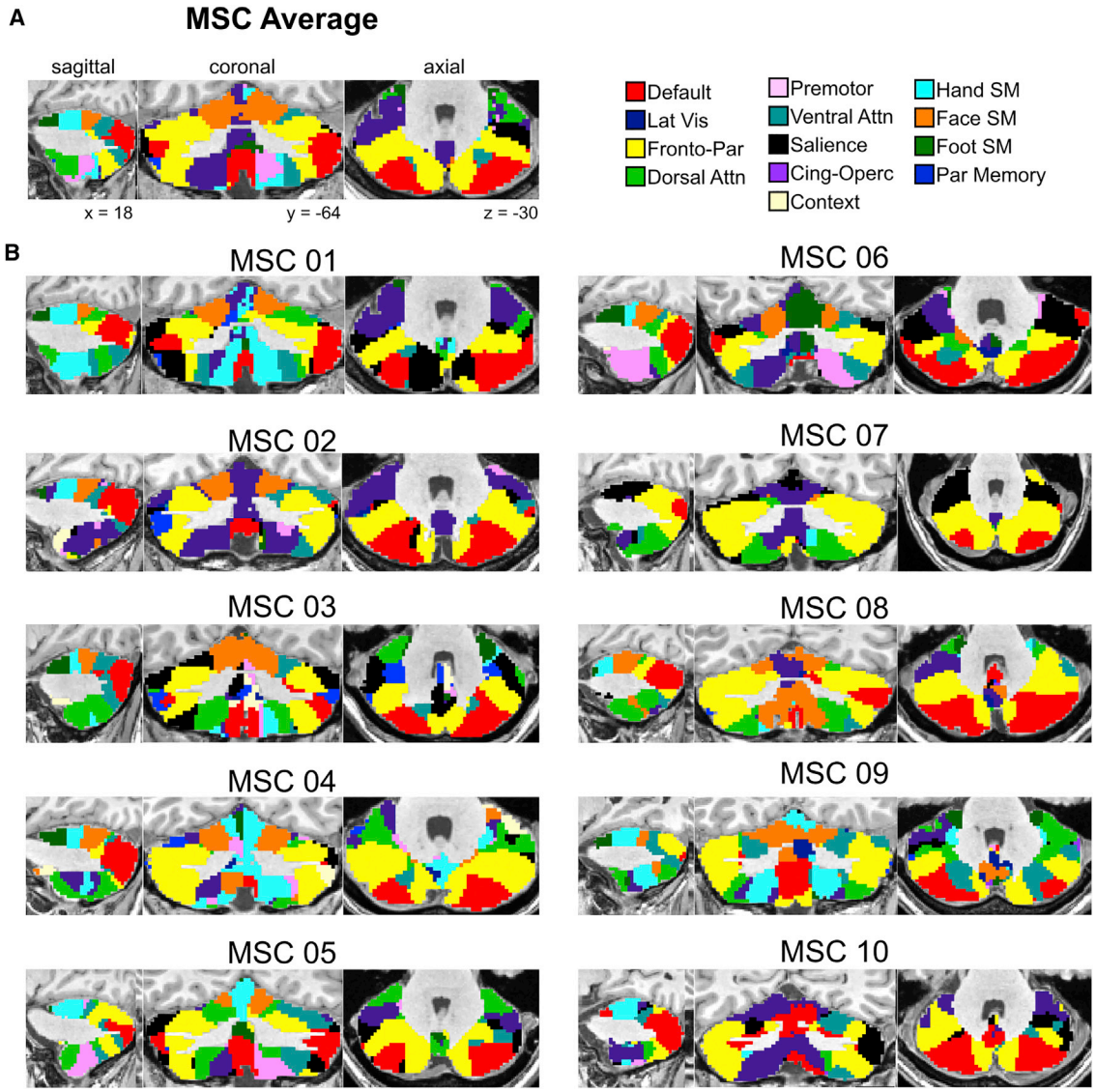


**Figure 1. Individual Cerebellar Networks Share Common Features with—and Deviate from—the Group Average**

(A) MSC average cerebellum winner-take-all network partitions.

(B) Individual MSC winner-take-all network partitions. Qualitatively, considerable variance exists between MSC subjects and between each subject and the group average.

were identified in the anterior cerebellum, running anterior-to-posterior, respectively. Control networks (frontoparietal and cingulo-opercular) demonstrated anatomically segregated representation along the anterior-to-posterior and medial-lateral axis, with the cingulo-opercular network represented medially in the anterior cerebellum, proximal to the motor networks, while the frontoparietal network was represented laterally and posteriorly. Similar to the control networks, the attention networks (dorsal attention and ventral attention) segregated along the A-P axis and had representations in both the dorsal and ventral cerebellum. The dorsal attention network was represented in the anterior cerebellum, whereas the ventral attention network was represented posteriorly, just posterior to the frontoparietal network. The default mode network was represented in the most medial posterior regions of the cerebellum, with additional representation in the flocculus. Replicating group average data (Buckner et al., 2011), visual and auditory networks were not represented in the cerebellum.

Although all subjects exhibited similar network organization, there were deviations across individuals from the group average in terms of specific positioning and relative amount of cerebellum dedicated to each network (Figure 1B). For example, some subjects demonstrated greater representation of the dorsal attention network, while others demonstrated greater representation of the cingulo-opercular network. In the posterior cerebellum (axial slices), there is considerable inter-subject variability

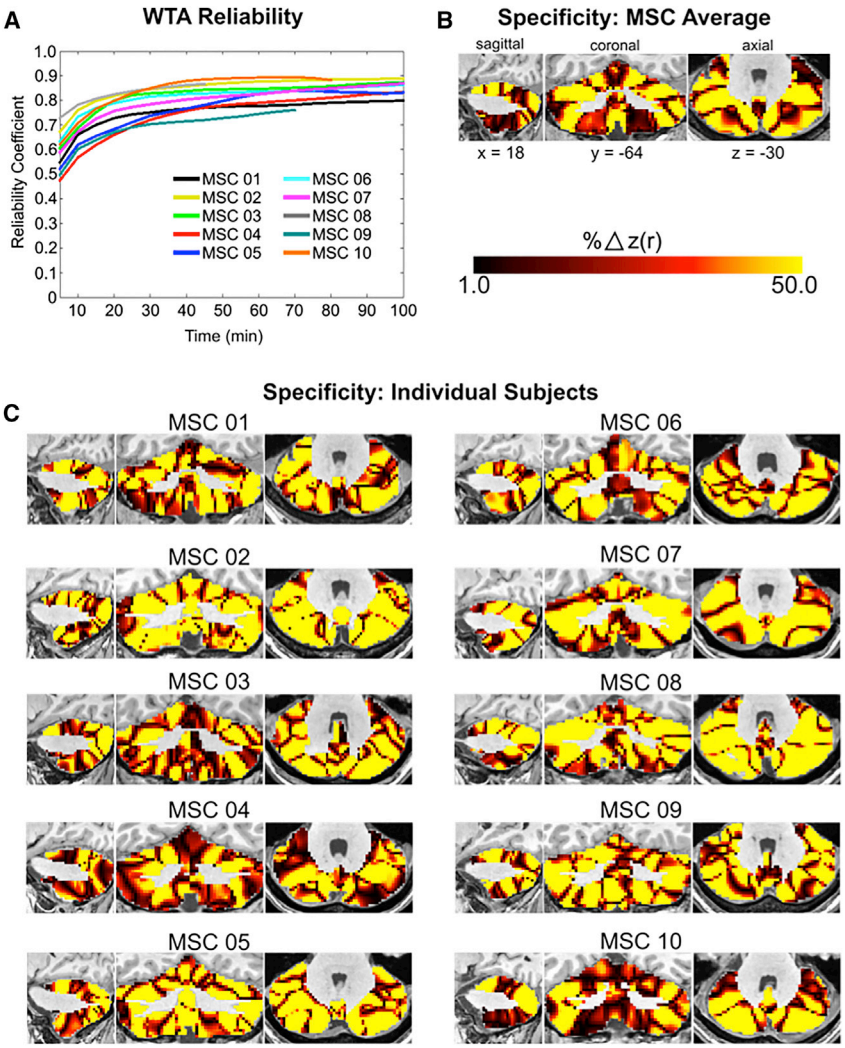


**Figure 2. Functional Networks Are Reliable with Sharp Individual-Specific Boundaries between Networks**

(A) The split-half reliability of individual subject WTA assignments increases with larger quantities of data. (B) MSC average percent difference in average correlation to cortical networks between the first place WTA assignment and the second place WTA assignment. (C) Percent difference in average correlation to cortical networks between the first place WTA assignment and the second place WTA assignment in each individual. Large differences in correlations between first and second place WTA assignments, coupled with high reliability ($\rho > 0.80$) resulting from large quantities of RSFC data, indicate networks are reliable and specific at the individual subject level.

in the placement of divisions between the default mode and frontoparietal networks. Within the motor network representations of the dorsal anterior cerebellum, individual differences in the representation of each motor network can be noted in the parasagittal slices. Thus, both common organization principles and individual differences existed in the WTA assignments between subjects and between each subject and the MSC average. Importantly, because WTA partitions are dependent on the underlying RSFC matrix that does not achieve good reliability until ~90 min of high-quality data have been acquired, large quantities of individual subject data are needed to achieve a stable estimate of individual cerebellar network organization.

## Functional Networks Are Reliable with Sharp Individual-Specific Boundaries between Networks

Despite achieving excellent RSFC reliability, one could argue the network partitions derived above might be spuriously variable between individuals due to the WTA method, which forces each voxel into a single "winning" network. To assuage these concerns, we calculated split-half reliability (see STAR Methods for details) on the WTA network assignments. On average, WTA network assignments required 90 min of post-motion censored RSFC data to achieve an average Spearman split-half correlation of 0.80 (Figure 2A). This quantity of data is equivalent to the quantities of data needed to delineate individual cortical networks (see Gordon et al., 2017c).

Given that the individual WTA partitions were as reliable as cortical networks from Gordon et al. (2017c), we tested for individual specificity in cerebellar networks by calculating the percent difference in average correlation (to the cortex) of the "first place" network and the "second place" network. By doing this, we were able to characterize which networks demonstrated a clear delineation between first and second place average RSFC with the cortex. On average, networks across the cerebellum demonstrated a clear delineation between first and second place networks, including both motor networks and—to an even greater extent—association networks, including the default mode and frontoparietal networks (Figures 2B and 2C), supporting the notion that single networks are reliably represented in many cerebellar voxels. Interestingly, the posterior cerebellum contained large representations of the premotor and cingulo-opercular networks, despite seeded correlations from primary motor cortex demonstrating strong connectivity to these same regions (see Figure S4 for cerebellar motor seed RSFC). Seed maps generated from posterior motor hand representations in the cerebellum revealed strong RSFC to cortical motor, premotor, and cingulo-opercular networks (Figure S5), providing evidence that the second representation of the cortex within the posterior cerebellum may be more integrative than the anterior representation.

## Strong Convergence between Individual Motor Activations and Functional Networks

We validated the claim that large quantities of data enabled accurate characterization of individual-specific motor subdivisions (i.e., foot, hand, face) within the cerebellum by leveraging 40 runs of a motor task per subject (STAR Methods) and determining the

convergence between resting state motor network partitions and motor foot, hand, and tongue task-evoked activity, separately. For every subject, we made a conjunction map within the cerebellum, overlapping task-evoked BOLD activity (for foot, hand, and tongue movements, separately) and WTA partitions (STAR Methods). Peak task-evoked BOLD activity in the cerebellum overlapped with individual WTA partitions in every subject across the three motor domains (Figure 3). Thus, precise partitioning of cerebellar motor networks is possible with large quantities of data.

## Individual-Level RSFC Variability in Network Organization Is Greater in the Cerebellum Than in the Cortex

Functional networks within the cortex are dominated by common organizational principles (group effects), as well as stable individual features (individual effects) that are differentially distributed across cortical networks (Gratton et al., 2018). Here, we similarly determined the contribution of group effects versus individual effects at the single-voxel/vertex level, as well as at the network level across individuals (STAR Methods). As shown in Figures 1 and S2, like cortical networks (Gratton et al., 2018), cerebellar networks appear to follow a similar mix of common organizational principles and individual specificity.

We computed the standard deviation of correlations across all voxels/vertices in the cerebellum and cortex (STAR Methods) to determine whether individual differences in cerebellar networks were more likely a result of greater between-subject variability in RSFC or actual individual-specific variability in cerebellar network topography. Inter-subject variance was significantly lower in the cerebellum (Figure 4A) compared to the cortex ($t = -3.77$, $p = 0.001$; Figure 4B), supporting the notion that there may be relatively larger group-level RSFC effects in the cerebellum than in the cortex. These results were replicated when we repeated this analysis in volume space (Pearson $r$ between approaches = 0.73). Additionally, between-subject variance was significantly greater in association networks compared to motor networks in both the cerebellum ($t = 4.01$, $p = 0.002$; Figure 4C) and cortex ($t = 2.98$, $p = 0.01$; Figure 4D), supporting greater individual-level RSFC variability in association networks.

Network-level group versus individual features were quantified directly by comparing the similarity of RSFC in resting state split-half sessions *between* subjects (group level) and similarity of RSFC in resting state split-half sessions *within* subjects (individual level) (Gratton et al., 2018). We directly quantified group-level (off-diagonal elements in Figure 4E) and individual-level effects (on-diagonal elements in Figure 4E) in RSFC and network organization in the cerebellum and compared these effects with the cortex in split-half portions of the dataset (STAR Methods). RSFC within the cerebellum demonstrated significantly greater group- and individual-level effects than RSFC within the cortex (group, $t = 4.26$, $p < 0.001$; individual, $t = 4.01$, $p < 0.001$; Figure 4F). The high level of group effects in the cerebellum (mean $z(r) = 1.09$; Figure 4F) and cortex (mean $z(r) = 0.99$) indicates that networks share a common organization across individuals. Networks from the same individual ("individual" effects) were even more similar to each other compared to the group in the cerebellum (added similarity of $z(r) = 1.12$; Figure 4F) and in the cortex (added similarity of $z(r) = 0.82$), indicating a clear influence of individual features over and above common organizational principles at the network level. Importantly, the larger similarity of individual effects within the cerebellum compared to cortex (difference in $z(r) = 0.40$) suggests cerebellar network organization may exhibit variability across subjects exceeding cortical network variability.

We tested for differences in the variability in the spatial arrangement of networks within the cerebellum and cortex across subjects via permutation testing (STAR Methods). Individual variability across subjects in the spatial arrangement of networks was significantly higher in the cerebellum than the cortex ($p < 0.0001$; Figure 5A). For quantification of anatomical overlap of each network across subjects, see Figure S6. Considerable RSFC variability existed in most networks across subjects, including both motor and association networks. Jointly, these results further support the finding that cerebellar network organization, though following gross common organizational principles, shows measurable variability between individuals. Furthermore, the lateral posterior lobes of the cerebellum, devoted to association networks, demonstrated the greatest level of inter-subject RSFC variability.

Previous work on precision mapping of individual cortical networks has shown convergence between task-evoked activity and network boundaries that varied anatomically between individuals along the precentral gyrus (Gordon et al., 2017c; Laumann et al., 2015). Similarly, we tested variability within the cerebellar motor system, taking two approaches. First, we quantified the amount of subject overlap in the convergence of task/rest for the somatomotor hand network (Figure 5B). The maximum anatomical overlap across subjects in the convergence between rest and task was seven out of ten subjects, supporting individual variability in hand motor representations. Second, the cerebellar voxel with peak activation during right hand movements (STAR Methods) was extracted for each subject (see Figures 5C and 5D for two individual subject examples). To depict overlap between resting state hand motor topography in the cerebellum and cortex within a subject (match) and non-overlap (mismatch) between subjects, we correlated the resting state time series of activity from this peak cerebellar voxel with every cortical vertex within each subject and to every other subject (see Figures 5C–5F for an example of two subjects and Figure 5G for all subjects). In eight out of ten subjects, peak task/rest overlap was higher within than between subjects; in the remaining two it was equal. In these two subjects (MSC 09 and MSC 10), peak task activity was anatomically near the group-average peak. As an example of the cerebellar mismatch in motor hand network overlap between subjects, within MSC 02, there was convergence between task and rest (Figure 5C), that overlapped with MSC 02's cortical hand motor network (Figure 5E, top row left). Conversely, the same voxel in MSC 06 lacks any strong correlation with MSC 06's cortical hand motor network (Figure 5E, bottom row left).

To provide additional quantification of the anatomical variability between individual subjects' hand motor representations in the cerebellum, we calculated the average Euclidean distance

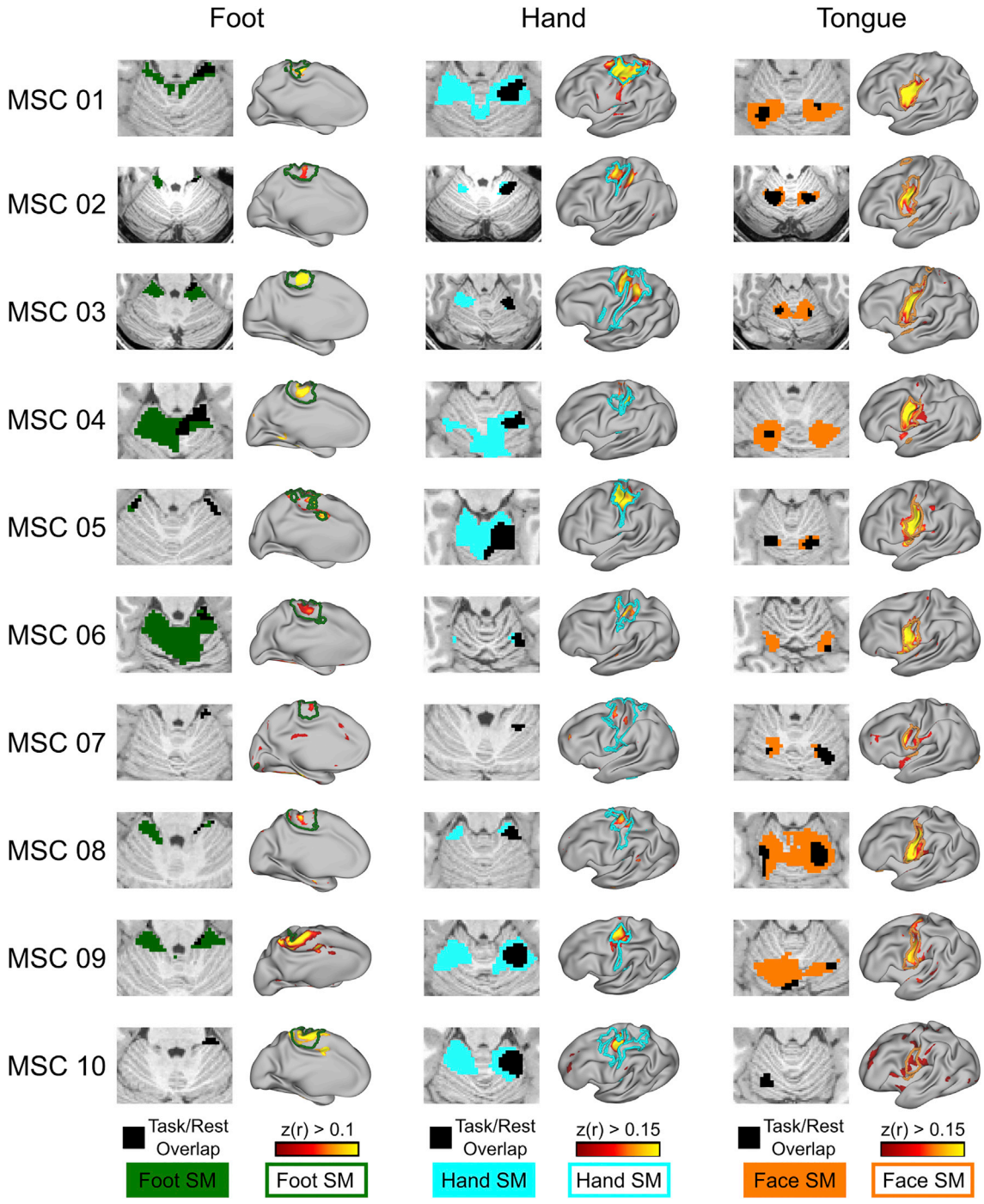


**Figure 3. Strong Convergence between Individual Motor Activations and Functional Networks**

Overlap between right motor foot, hand, and tongue task-evoked BOLD activity and their respective resting state RSFC overlaid on WTA partitions in the cerebellum (colored patches). Note the laterality of the overlap. The black patch represents the overlap between the task and resting state. More specifically, in the resting state data, we placed a seed in an area of motor cortex that demonstrated the greatest task-evoked activity across trials of a given movement (foot, hand, and face, separately). This map was then thresholded at $r > 0.10$. Next, we correlated the cerebellar task time series with this cortical motor seed (beta series correlation) and thresholded this map at $r > 0.10$. Seeded correlation from cerebellar voxel demonstrating the greatest task-evoked activity to the cortex. Colored outline denotes Infomap-derived cortical network borders.

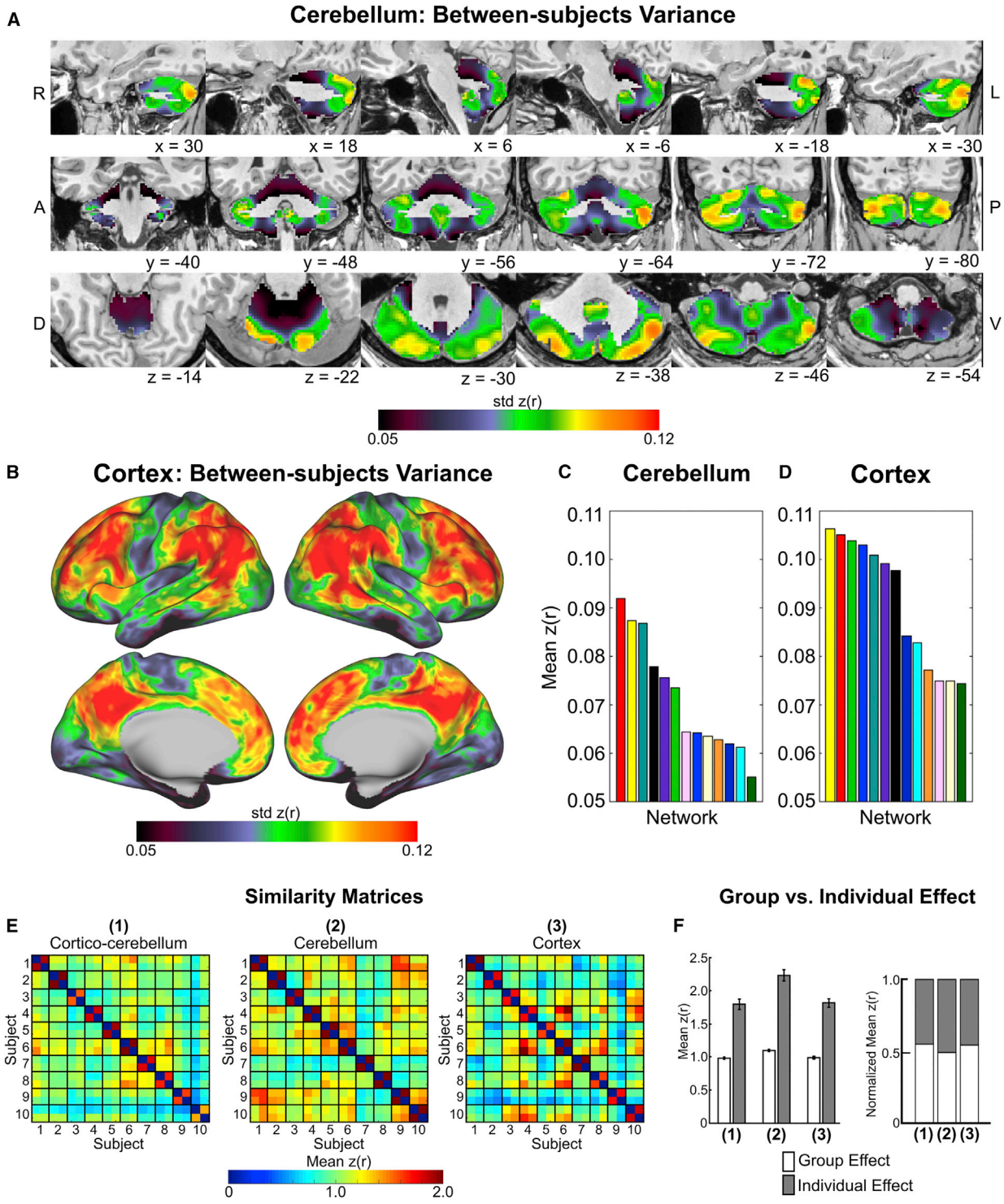


**Figure 4. Network-Level RSFC Individual Effects Are Greater in the Cerebellum Than in the Cortex**

(A and B) Between-subject variance topography in the (A) cerebellum and (B) cortex.

(C and D) Between-subject variance was greater in cognitive networks compared to motor networks and smaller in the cerebellum (C) than in the (D) cerebrum.

(E) Network similarity matrices. Off-diagonal elements represent group effects, whereas on-diagonal elements represent individual effects.

(F) Quantification of group versus individual effects for RSFC (1) between the cerebellum and cortex, (2) within the cerebellum, and (3) within the cortex. Error bars denote SEM across subjects.

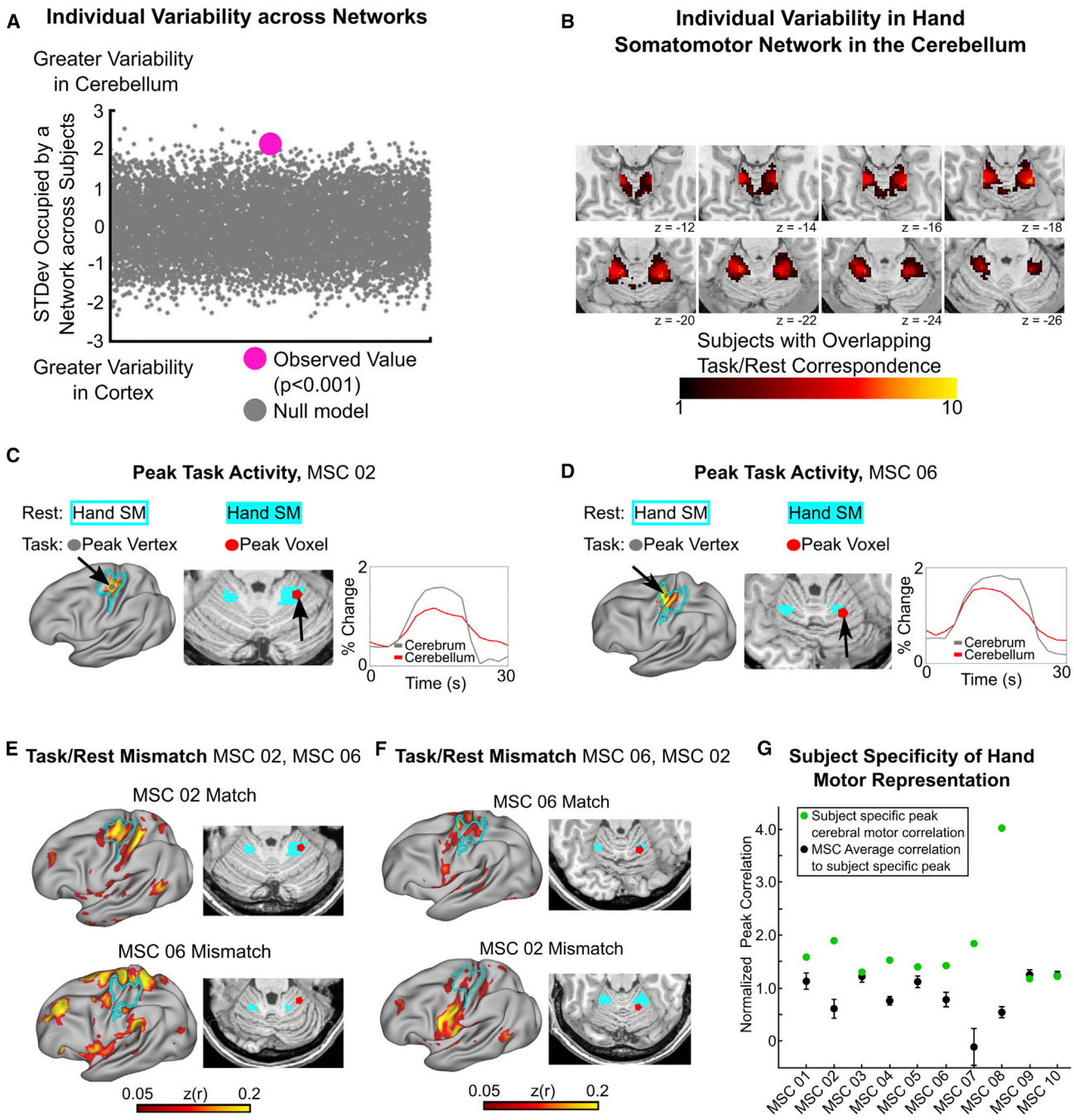


**Figure 5. Individual Variability in Network Organization Is Greater in the Cerebellum Than in the Cortex**

(A) Difference across subjects in the standard deviation of the quantity of total space occupied by a network in the cerebellum versus the cortex. Positive values indicate greater between subject variability in network organization within the cerebellum.

(B) Overlap across subjects in individual-specific convergence between task and rest. Higher numbers indicate greater overlap between subjects. Note that no voxels within the cerebellum contain overlap across all ten individuals.

(C and D) Single vertex/voxel peak activation during right hand movement falls within resting state hand somatomotor network in both the cortex (left panel; gray node within cyan outline) and cerebellum (middle panel; red node within cyan patch), and demonstrates a highly correlated time series of activation in individual subjects. Note the persistence of the cerebellar response compared to the cortical response.

(E) RSFC from cerebellar voxel from (C) (MSC 02) to the cortex converges on MSC 02's resting state cortical hand somatomotor network (top row), but not another MSC subject (MSC 06; bottom row).

*(legend continued on next page)*

between an individual subject's task/rest overlap voxels (peak voxels for each subject in Figure 5G). The average Euclidean distance across subjects was 8.2 mm with a standard deviation of 4.5 mm. Altogether, the critical implication regarding the high level of individual variability in RSFC is that group-average studies are spatially misrepresenting portions of individual subject networks within the cerebellum.

### The Frontoparietal Network Is Disproportionately Expanded in the Cerebellum Compared to Cortex

The WTA, similarity, and variability analyses above provided evidence for both common, group-level organizational principles and individual specificity of cerebellar networks. To probe these spatial organization principles further and determine the degree of consistency between network representations in the cerebellum and cortex, we determined the percent of the total cerebellar volume occupied by each network and percent of the total cortical surface area occupied by each network. On average, association networks occupied 80.2% of total cerebellar volume, whereas premotor and motor networks occupied 19.8% of total cerebellar volume (Figure 6A, top row). By comparison, association networks occupied 64.8% of the cortical surface area, whereas premotor and motor networks occupied 19.8% of the cortical surface area (Figure 6B). Visual and auditory networks occupied the other 15.4% of the cortical surface areas. We further quantified cerebellar network proportions in anterior and posterior cerebellar lobes. This analysis revealed a slightly different proportion of association networks in the anterior cerebellum (76%) compared to the posterior cerebellum (85%).

Unlike all other networks, the frontoparietal network was disproportionately expanded in the cerebellum, such that it had a 2.3-fold greater relative representation in the cerebellum compared to the cortex (Figures 6C and 6D). Importantly, the greater representation of the frontoparietal network in the cerebellum compared to the cortex was consistent across every individual. Across all MSC subjects, the frontoparietal network occupied 23.17% of the total cerebellar volume, whereas it only occupied 10.13% of total cortical surface area. This 2.3-fold overrepresentation of the frontoparietal network was maintained or estimated as high as 3-fold when we did not include voxels with low signal-to-noise ratio (tSNR < 2.5), low specificity (<50% in Figure 2), or relatively low voxel-wise reliability ($r < 0.70$) (Figure S7), supporting previous group-average quantification of frontoparietal representations in the cerebellum versus cortex (Buckner et al., 2011). The total cerebellum volume dedicated to the frontoparietal network was greater than all of the cerebellar motor and premotor networks combined. Moreover, the frontoparietal network contains the largest absolute representation of any network in the cerebellum and cortex. Despite the cerebellum's common characterization as a motor structure, 80% of the cerebellum is occupied by networks contributing to top-down regulatory functions.

### Cerebellar BOLD Signals Systematically Lag Cortical BOLD Signals

The cerebellum was found to be dominated by association networks. Yet, how cortico-cerebellar networks are organized temporally is unclear. Previous analyses of regional delays among BOLD time series have implicated propagation of spontaneous ISA on the order of 1 s both within and between canonical functional networks (Mitra et al., 2014, 2015). However, the network-level relationship—as well as degree of individual specificity and variability—in the temporal organization of spontaneous fluctuations between the cerebellum and the cortex remains unknown.

We adopted a previously described cross-covariance approach to lag estimation in fMRI data (Mitra et al., 2014, 2015) to characterize temporal relationships between the cortex and cerebellum. Pairwise temporal relationships can be visualized via a time delay (TD) matrix, in which each element represents the average latency between the time series of two regions. We constructed such matrices to include both cortical vertices and cerebellar voxels for each individual and the MSC average. The portion of Figure 7A outlined in light gray displays the MSC average TD matrix, corresponding to cortical vertices, after organizing by network affiliation and temporally sorting from early to late within each network. Note that even off-diagonal blocks within the cortex have both early and late portions, reaffirming the apparent between-network propagation described previously (Mitra et al., 2014, 2015). We repeated this procedure for all cerebellar voxels. Although some within- and between-network propagation is observed in the diagonal and off-diagonal blocks within the cerebellum (outlined in dark gray), respectively, the magnitude is less than in the cortex. This indicates there is little to no systematic temporal organization in the propagation of ISA *within* the cerebellum.

Given the presence of cortico-cerebellar loops, and their purported role in error signaling and adaptive plasticity, we were particularly interested in the temporal organization of ISA *between* the cerebellum and cortex. As can be seen in the portion of Figure 7A outlined in black, the vast majority of pairwise cortico-cerebellar relationships were positive, indicating cerebellar BOLD signals temporally lagged cortical BOLD signals. We proceeded to compute, for each cerebellar voxel, its mean latency across all cortical vertices. The resulting latency map of the cerebellum, a cerebellum-cortex-specific "lag projection" (Mitra et al., 2014), reflects the average latency of each cerebellar voxel with respect to the cortex (mean of Figure 7A outlined in black). In these lag projections, every cerebellar voxel, in each subject (Figure 7C) and the group average (Figure 7B), had a temporally lagged (positive) value. Mean latency values within cerebellar association networks ($M = 286$ ms, SD = 145 ms) were significantly later than cerebellar motor networks ($M = 124$ ms, SD = 63 ms) in both the MSC average ($t = 61.84$, $p < 0.0001$) and each individual (all $t > 4.51$, all $p < 0.0001$) (Figures 7B and 7C). To test whether

(F) RSFC correlation from cerebellar voxel from (D) (MSC 06) to the cortex converges on MSC 06's resting state cortical hand somatomotor network (top row), but not another MSC subject (MSC 02; bottom row).

(G) The mean correlations from a given subject's peak task activation within the cerebellum to the hand somatomotor cortex was higher than within other subjects from the same cerebellar voxel, indicating individual specificity. Error bars denote SEM across the nine other subjects.

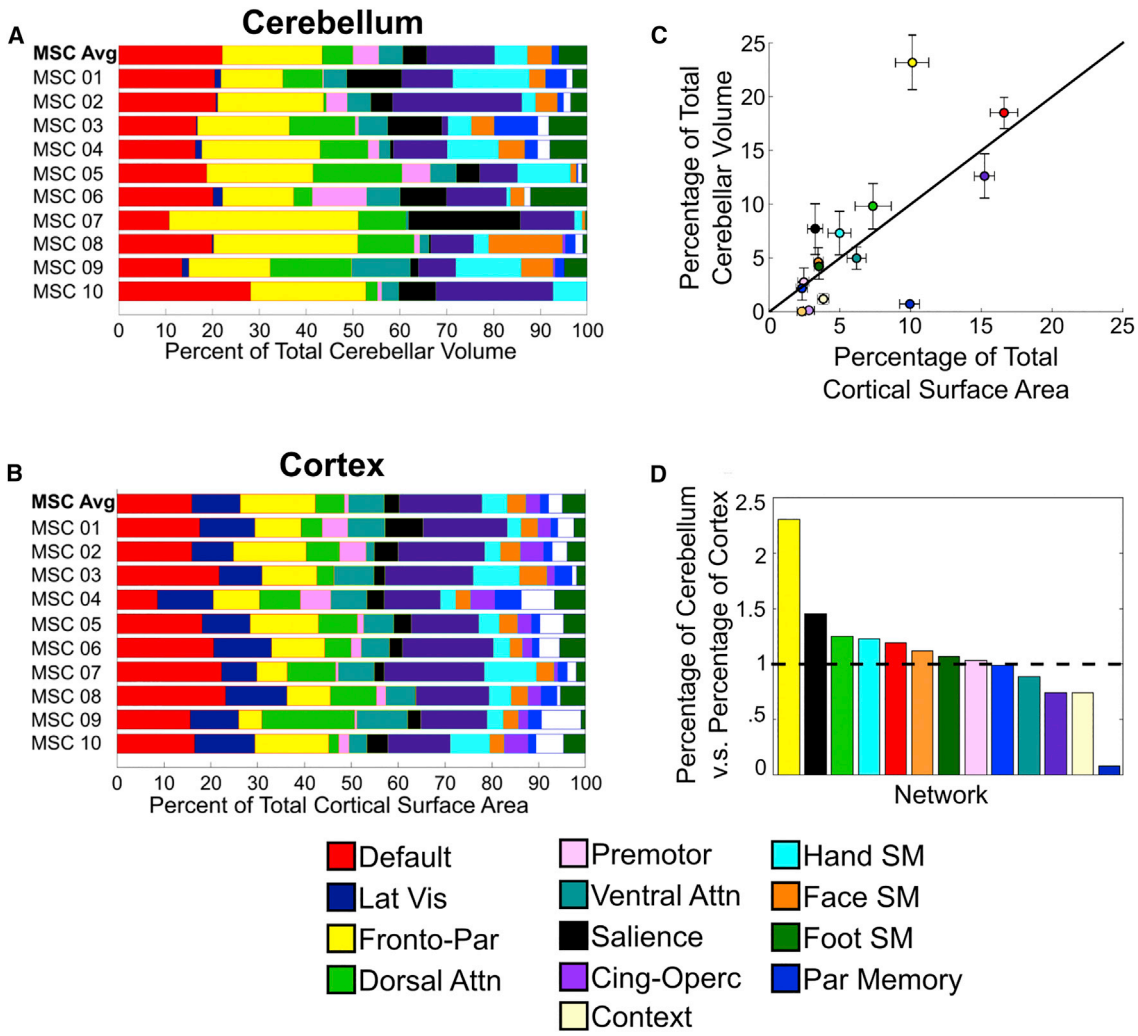


**Figure 6. The Frontoparietal Network Is Disproportionately Expanded in the Cerebellum Compared to the Cortex**

(A and B) Network representation (percent of total volume/surface occupied by a network) was quantified in the cerebellum (A) and cortex (B).

(C) Percentage of total surface area (cortex) relative to percentage of volume (cerebellum) for each network. Black line represents identity line (i.e., equal representation in the cerebellum and cortex). Error bars represent the SEM across subjects. The frontoparietal network occupies more space in the cerebellum than any other network.

(D) Relative ratio (cerebellum/cortex) of network representation. Values greater than one (horizontal dotted line) indicate greater relative space occupied by a network in the cerebellum, whereas values less than one indicate greater space occupied by a network in the cortex.

proximity to major draining veins could be affecting the cerebellar lags, we recalculated the mean lag of each network in the anterior cerebellum (more distant from veins) versus the posterior cerebellum (closer to veins) and did not find a difference across networks (Cohen's $d$ = 0.02; Table S1 for each subject and network) Thus, *all* cerebellar BOLD signals lag cortical BOLD signals systematically and consistently across all subjects.

## DISCUSSION

Precision functional mapping of the human cerebellum revealed that (1) individual maps of cerebellar network organization are reliable and exhibit common group-level organizational principles, as well as individual-specific features; (2) individual variability of the spatial arrangement of networks is greater in the cerebellum than in the cortex; (3) the frontoparietal network, thought to support adaptive control, is overrepresented in the cerebellum compared to the cortex across every individual; and (4) the cerebellum temporally lagged the cortex systematically, such that association networks within the cerebellum demonstrated greater mean latency (lag) from the cortex than motor networks within the cerebellum. Jointly, these results provide evidence that the human cerebellum is dominated by association networks particularly the frontoparietal network—that demonstrate both common group-level spatiotemporal organization and individual-specific spatial arrangement.

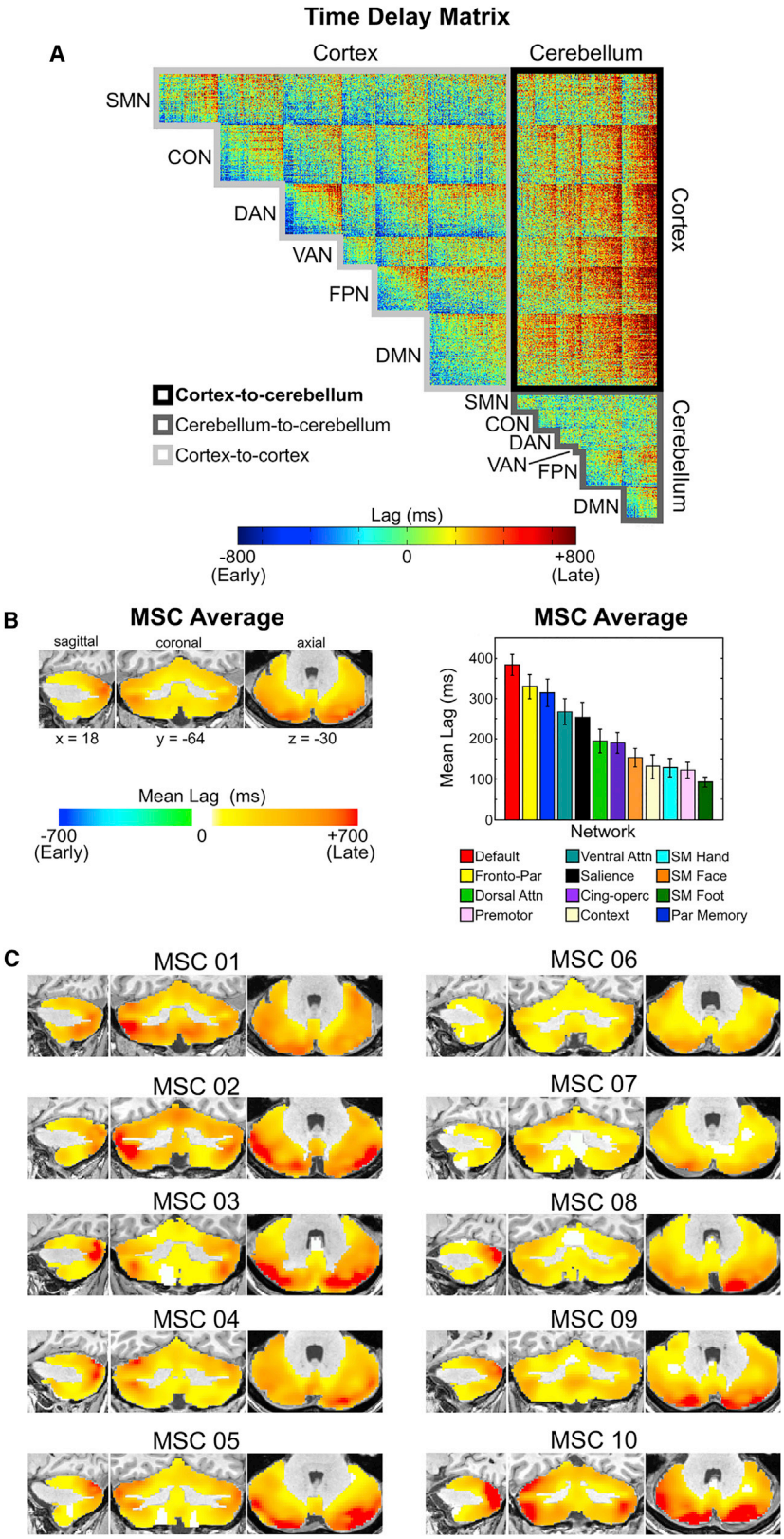


**Figure 7. Cerebellar ISA Systematically Lags Cortical ISA**

(A) MSC average time delay matrix. Note the degree to which cerebellar BOLD signal lags behind the cortex compared to cortico-cortical signals or cerebello-cerebellum signals.

(B) Average temporal lag of each cerebellar voxel relative to all cortical vertices in the MSC average, quantified by network. This lag projection is computed as an average along each column of the "Cortex-to-cerebellum" portion of the time delay matrix. Note that ISA within every voxel in the cerebellum, on average, lags behind ISA in the cortex. Error bars denote SEM.

(C) Average lag in ISA between each cerebellar voxel and all cortical vertices in individual subjects.

### Reliable, Individual-Specific Cerebellar Functional Network Topography Can Be Elucidated with Large Quantities of Data

Previous studies utilizing an individual precision functional mapping approach demonstrated that hours of data per individual enabled the description of systematic and reliable individual differences in cortical network topography (Gordon et al., 2017c; Laumann et al., 2015), obscured by group averaging. Here, we demonstrated this same principle holds for cerebellar functional organization, but with the requirement of even larger amounts of data. Specifically, RSFC in the cerebellum achieved an equivalent level of excellent reliability ($r > 0.90$ with respect to the cortex) with 90 min of low-motion data. As in the cortex, individual motor homunculi (foot, hand, and face) representations were demonstrated in each subject (Figure 3), and were shown to vary anatomically across the dorsal anterior cerebellum (Figure 5).

One nuance of delineating network organization in the cerebellum versus the cortex is the partitioning approach in obtaining discrete networks. Consensus approaches to derive networks in the cortex, such as Infomap, often need to be modified in the striatum (Choi et al., 2012; Greene et al., 2014), thalamus (Hwang et al., 2017), and cerebellum (Buckner et al., 2011), using a WTA approach with the cortex as a template. Although these previous studies used large group-averaged datasets, given their success in delineating reliable network partitions in subcortical structures, we elected to take a similar WTA approach here. With large quantities of data (90 min to achieve $\rho > 0.80$), the WTA approach results in reliable, individual-specific networks that converge with task data and follow sharp boundaries between networks.

For a given quantity of data, relatively lower reliability in the cerebellum compared to the cortex could be due to factors relating to noise and/or differences in the BOLD signal. Generally, signal-to-noise ratio is lower in the subcortex and cerebellum and these regions are susceptible to artifacts, which would lead to poorer reliability for a given quantity of data in the cerebellum compared to cortex. Interestingly, there are numerous distinguishing features of the cerebellum that may systematically affect BOLD signal reliability. The cerebellum contains four times more neurons than the cortex, but very few glia, including astrocytes. Purkinje cells, which are the main output cells of the cerebellum, are inhibitory, whereas cortical pyramidal cells are excitatory. The cerebellum contains ~40–50 billion granule cells, which are not present in the cerebral cortex. Metabolically, the cerebellum largely does not utilize aerobic glycolysis, while the cerebral cortex does, especially within the default mode network (Vaishnavi et al., 2010). One or more of these differences in cellular architecture and/or metabolism may contribute to differences in reliability of the BOLD signal measured during the resting state.

### Cerebellar Networks Are More Variable Than Cortical Networks across Individuals

Recently, it was discovered that networks within the cortex are dominated by common organizational principles and stable individual topography, with far less modulation as a function of day-to-day variability and task state (Gratton et al., 2018). Given the stability of individual features, one provocative implication from this study is that resting state fMRI offers promising utility in characterizing individual variability in brain/behavior relationships and furthering our understanding of neurological and psychiatric disorders. While previous group-average studies have advanced our understanding of the brain regions and networks implicated in a broad range of disorders (Greene et al., 2016), the lack of attention to these stable individual features likely is impeding progress in understanding the etiology and treatment of neurological and psychiatric disorders.

We found evidence that RSFC and network organization within the cerebellum exhibit common organizational principles and individual variability that is greater than the cortex. While the large group effect within the cerebellum (Figure 4E) supports the idea that important information can be gleaned from group-average studies (Buckner et al., 2011), the even larger individual effects in RSFC emphasize the need for complementary approaches to human functional imaging studies of the cerebellum in both typical and atypical cohorts.

The cerebellum has been implicated in the emergence of several psychiatric disorders, including autism (Marko et al., 2015), attention deficit hyperactivity disorder (Tomasi and Volkow, 2012), and schizophrenia (Chen et al., 2013). Clinical studies have shown that cerebellar damage results in individual-specific impairments, including in task-switching, associative learning, and reasoning (Schmahmann and Sherman, 1998). Given the relatively larger level of individual specificity in the cerebellum compared to cortex, accurate spatial and temporal RSFC characterization of psychiatric disorders would likely benefit from whole-brain approaches.

### The Frontoparietal Network, Critical for Adaptive Control, Is Disproportionately Expanded in the Cerebellum Compared to the Cortex

Consistent with previous group-average studies (Buckner et al., 2011), the frontoparietal network was overrepresented 2.3-fold in the cerebellum compared to the cortex, occupying more cerebellar volume than any other resting state network. Why is so much of the human cerebellum devoted to a network supporting adaptive control? We contend it is the result of disproportionate expansion of the lateral cerebellum in humans, supporting the impressive repertoire of adaptive capabilities with which we are privileged. The frontoparietal network supports task set initiation and task switching, regulating the integration of other association and motor networks (Dosenbach et al., 2007). Cerebellar damage to the lateral posterior lobes, occupied by the frontoparietal network, often leads to cerebellar cognitive affective syndrome (Schmahmann and Sherman, 1998), with disturbances to a broad range of control functions, including task switching, working memory retrieval, visuo-spatial integration, language, and an overall reduction in intellectual function (Schmahmann, 2004).

Comparison between human and non-human primates has provided additional evidence that the disproportionate expansion of the lateral cerebellum supports adaptive control. Humans can implement rapidly switching abstract rule sets with minimal verbal instruction and training. This is not the case for non-human primates, which require exhaustive training to perform operations mimicking task switching. Evidence suggests macaques incur little to no switch cost, but they experience high task

interference cost during task switching, while humans incur switch costs even with training and small interference cost (Stoet and Snyder, 2003). As such, human and non-human primates differ markedly in frontoparietal network regulatory processes supporting task switching. The disproportionate representation of the frontoparietal network within the cerebellum may be pivotal for rapid adaption capabilities of humans. While we were not powered to detect brain/behavior relationships (Gordon et al., 2017c), an important future direction will be to collect high-fidelity RSFC data on larger samples to understand the specific individual effects that contribute to individual differences in behavior and disease.

## Contributions of the Cerebellum to Individual-Specific Adaptive Plasticity

In contrast to its conserved cytoarchitecture across species (Caligiore et al., 2017), cerebellar contributions to behavior are vastly different across mammalian species, suggesting that the cerebellum links to species-specific systems. For example, unlike humans, the cerebellum in whales has largely expanded in the paraflocculus, supporting echolocation and acoustic communication (Oelschlager, 2000). Similarly, the rat paraflocculus receives inputs from primary auditory cortex via the pons (Azizi et al., 1985). The rat cerebellum modulates cortico-striatal plasticity through reciprocal connections with the basal ganglia (Chen et al., 2014) and modulates cortical sensorimotor integration (Popa et al., 2013). In humans, non-invasive stimulation studies demonstrated that cerebellum output modulates primary motor cortex plasticity, suggesting polysynaptic connections between the cerebellum and cortex support the rapid adaptation to novel environmental challenges during movement planning (Caligiore et al., 2017).

The cerebellum also may play a critical role in cortical plasticity and adaptation of higher-order constructs, such as language (Thach, 2007). Human imaging studies of healthy subjects have demonstrated increased functional connectivity between the lateral cerebellum and the frontoparietal network soon after sensorimotor learning (Albert et al., 2009) and after a period of learning the serial reaction time task (Sami et al., 2014). In human adults left hemisphere dominant for speech, left cortical hemisphere damage results in a period of little to no speech, followed by a gradually regaining of speech. Imaging of these individuals during speech has shown that right cortical hemisphere activity increases along with the *left* cerebellar hemisphere, reverse of typical right cerebellar increased activity in language tasks (Connor et al., 2006). The cerebellum also has been shown to undergo morphological changes after a 100-day cognitive training program (Raz et al., 2013). These studies suggest the cerebellum may play a role in modulating the cortex in an experience-dependent manner, supporting individual-specific plasticity.

Given cerebellar individual variability and contributions of the cerebellum to experience-dependent plasticity, we posit the cerebellum may be an especially plastic structure important to neurodevelopment. Functional networks supporting the maturation of control demonstrate a protracted development throughout adolescence and adulthood (Grayson and Fair, 2017; Luna et al., 2015; Marek et al., 2015). Given the frontoparietal network's role in adaptive control and disproportionate representation within the cerebellum, the lateral cerebellum may be an overlooked source of experience-driven learning that contributes to cognitive maturation. Developmental studies focusing on the consequence of cerebellar damage support the notion that the cerebellum supports both motor and cognitive maturation. In some children, resection of cerebellar tumors results in posterior fossa syndrome, characterized by mutism, dysarthria, disengagement of any spontaneous movement, and marked personality changes including apathy and rapid fluctuations of emotions (Schmahmann, 2004). Children with cerebellar agenesis or partial lesions, both motor and cognitive milestones, are delayed and some individuals present with general intellectual disabilities (Gardner et al., 2001). Thus, damage to the cerebellum often results in prominent motor and cognitive deficits that are on par with, or even exceed, damage to the cortex.

The uniform cytoarchitecture of the cerebellum suggests a common computation is occurring in each cerebellar module, potentially engaging in a ubiquitous function of providing the automatic correction to all cortical output. As such, cerebellar insults may lead to "dysmetria" in the functioning of whichever functional network is implicated (Schmahmann, 2004). Future studies are needed to test this hypothesis, coupling rigorous neuropsychological testing with precision mapping of individual humans.

## A Model of Cortico-Cerebellar Temporal Propagation

BOLD signals in the cerebellum lagged behind BOLD signals in the cortex by 100–400 ms in a network-specific manner that was reproducible across all 10 subjects. Specifically, motor network BOLD activity lagged behind cortical BOLD activity by ~125 ms, while association network BOLD activity lagged behind cortical BOLD by ~280 ms. The TD matrix of Figure 7A suggests that, for each of the functional networks that are represented in both the cortex and cerebellum, the cerebellar portion of the network represents the final destination for spontaneous ISA propagating through the network. This is consistent with a model in which cortical output is processed in the cerebellum via polysynaptic anatomical connections from the cortex before being relayed back to the same cortical areas, supporting the cerebellum's role in supervised learning and adaptation, and error signaling (Dosenbach et al., 2006; Fiez et al., 1992).

It was recently discovered that ISA (0.01–0.10 Hz) and delta band (0.5–4 Hz) activity propagate in opposite directions between the hippocampus and cerebral cortex (Mitra et al., 2016). Using wide-field optical calcium/ hemoglobin imaging and laminar electrophysiology in mice, it was discovered that reciprocal propagation of ISA and delta activity occurs across the cerebral cortex (Mitra et al., 2018). Additionally, the phase of ISA was coupled with the amplitude of delta activity, suggesting that ISA may structure higher frequency activity, as predicted by theories of neural communication via phase-amplitude coupling (Fries, 2015). Based on the present findings, we hypothesize that cortico-cerebellar loops exhibit a similar frequency-specific temporal organization (Figure 8). In this model, cerebellar ISA lags cortical ISA in a network-specific fashion. Based on evidence for reciprocal propagation of ISA and delta band activity in the cortex, we speculate a similar spatiotemporal organization exists in cortico-cerebellar loops. Within these loops, ISA originating in the cortex temporally organizes higher

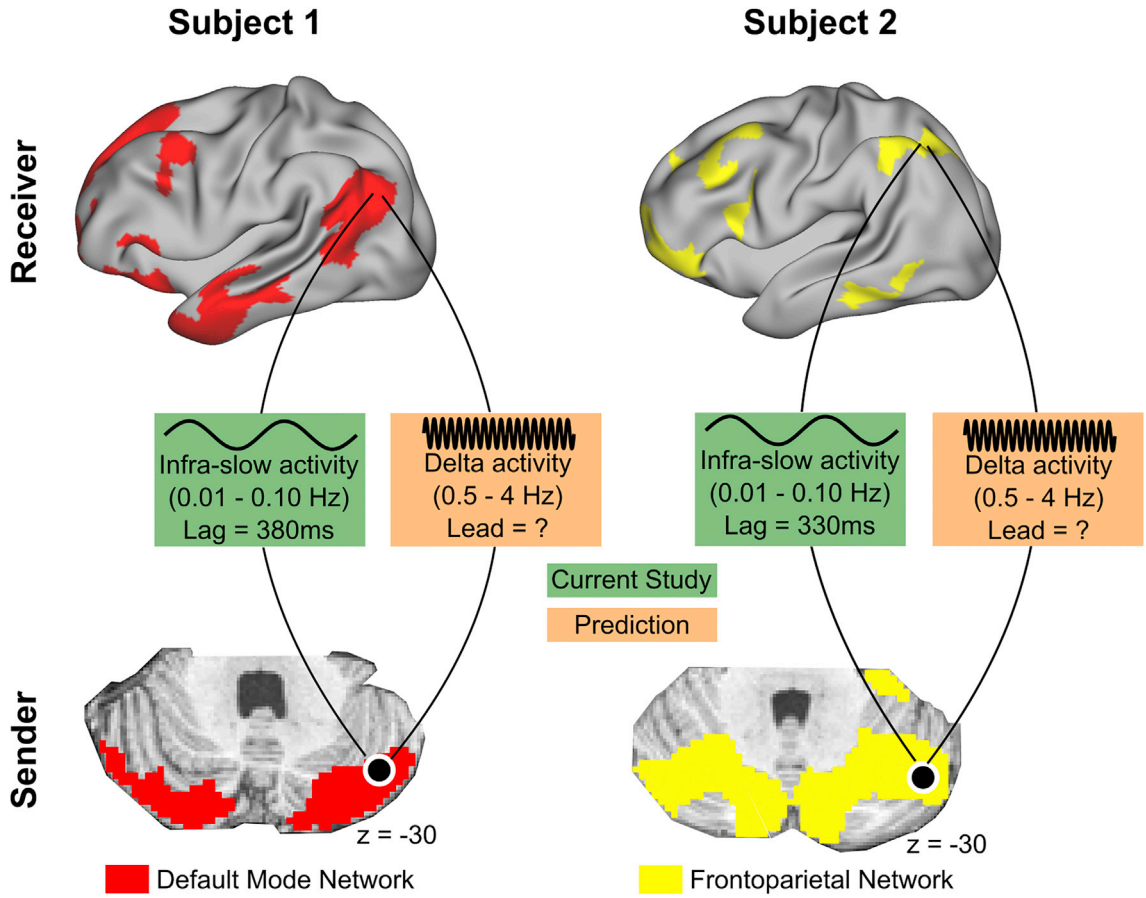


**Figure 8. A Model of Cortico-Cerebellar Temporal Propagation**

Cerebellar ISA lags cortical ISA in a network-specific fashion. ISA paces higher frequency activity, providing windows of opportunity for the sender (cerebellum) to transmit information to the receiver (cortex). High-fidelity data are required to accurately delineate cortico-cerebellar loops, since the same anatomical location in two individuals may be part of different functional network loops.

frequency activity originating in the cerebellum, providing windows of opportunity for the cerebellum (sender) to transmit information to the cortex (receiver). Accurate characterization of individual-specific cerebellar networks is required to accurately map cerebro-cerebellar circuits, as the same anatomical locus within the cerebellum may result in different cortico-cerebellar network loops (as is the case between Subject 1 and Subject 2 in Figure 8). Delays in ISA may vary by network due to the time it requires the cortex (receiver) to integrate information sent from the cerebellum. Future electrophysiological studies are needed to directly test these predictions. Interestingly, some recent evidence suggests stimulation of cerebellar outputs using delta frequency optogenetics rescues attenuated medial prefrontal cortex activity in a mouse model of schizophrenia, indicating delta band cerebellar activity may be an important frequency regime in modulation of cortex (Parker et al., 2017).

## Conclusion

Using the high-fidelity MSC dataset, we mapped the spatial and temporal organization of cerebellar functional networks in ten individuals. Using 5 hr of resting state data per subject, we found that the cerebellum is functionally characterized by common, group-level organizations principles, as well as individual-specific features. Individual variability in the spatial arrangement of functional networks was significantly greater than in the cortex. The frontoparietal network, critical for adaptive control, was the only network overrepresented in the cerebellum compared to the cortex (2.3-fold). Temporally, all cerebellar resting state signals lagged behind the cortex (125–380 ms), most prominently within association networks. Both of these group-level effects were evident in all ten individuals. These combined group level and individual level findings suggest a domain-general function of the cerebellum may be the ultimate correction of all cortical motor and cognitive processes.

## STAR★METHODS

Detailed methods are provided in the online version of this paper and include the following:

- KEY RESOURCES TABLE
- CONTACT FOR REAGENT AND RESOURCE SHARING

## SUPPLEMENTAL INFORMATION

Supplemental Information includes seven figures and one table and can be found with this article online at https://doi.org/10.1016/j.neuron.2018.10.010.

## ACKNOWLEDGMENTS

This work was supported by NIH grants 5T32 MH100019-02 (S.M.), NS088590 (N.U.F.D.), TR000448 (N.U.F.D.), MH100872 (T.O.L.), MH109589 (D.M.B.), MH104592 (D.J.G.), 1P30NS098577 (to the Neuroimaging Informatics and Analysis Center), and HD087011 (to the Intellectual and Developmental Disabilities Research Center at Washington University); the Jacobs Foundation grant 2016121703 (N.U.F.D.); the Child Neurology Foundation (N.U.F.D.); the McDonnell Center for Systems Neuroscience (N.U.F.D. and B.L.S.); the Mallinckrodt Institute of Radiology grant 14-011 (N.U.F.D.); the Hope Center for Neurological Disorders (N.U.F.D., B.L.S., and S.E.P.); and Dart Neuroscience LLC (K.B.M.). The views expressed in this article are those of the authors and do not necessarily reflect the position or policy of the Department of Veterans Affairs or the U.S. government.

## AUTHOR CONTRIBUTIONS

Conceptualization, S.M., J.S. Siegel, E.M.G., D.J.G., and N.U.F.D.; Methodology, Software, and Formal Analysis, S.M., J.S. Siegel, E.M.G., R.V.R., D.J.N., M.O., T.O.L., B.A., D.B.M., A.Z., C.G., A.L.N., D.D., A.N.V., M.E.R., S.E.P., D.J.G., and N.U.F.D.; Data Curation and Processing, E.M.G., D.J.N., M.O., T.O.L., J.J.B., C.R.H., K.B.M., R.S.C., D.J.G., and N.U.F.D.; Writing – Original Draft, S.M., J.S. Siegel, E.M.G., R.V.R., D.J.N., C.G., D.D., S.A.N., J.S. Shimony, A.Z.S., S.M.N., D.M.B., B.L.S., M.E.R., S.E.P., D.J.G., and N.U.F.D.; Writing – Review & Editing, S.M., J.S. Siegel, E.M.G., R.V.R., D.J.N., M.O., T.O.L., K.C.L., C.G., J.J.B., R.S.C., D.D., S.A.N., J.S. Shimony, A.Z.S., S.M.N., D.M.B., B.L.S., M.E.R., S.E.P., D.J.G., and N.U.F.D. Supervision, B.L.S., M.E.R., S.E.P., D.J.G., and N.U.F.D.

## DECLARATION OF INTERESTS

The authors declare no competing interests.

Received: April 27, 2018
Revised: August 13, 2018
Accepted: October 5, 2018
Published: October 25, 2018

## REFERENCES

Albert, N.B., Robertson, E.M., and Miall, R.C. (2009). The resting human brain and motor learning. Curr. Biol. *19*, 1023–1027.

Andersen, B.B., Korbo, L., and Pakkenberg, B. (1992). A quantitative study of the human cerebellum with unbiased stereological techniques. J. Comp. Neurol. *326*, 549–560.

Azizi, S.A., Burne, R.A., and Woodward, D.J. (1985). The auditory corticopontocerebellar projection in the rat: inputs to the paraflocculus and midvermis. An anatomical and physiological study. Exp. Brain Res. *59*, 36–49.

Balota, D.A., Yap, M.J., Cortese, M.J., Hutchison, K.A., Kessler, B., Loftis, B., Neely, J.H., Nelson, D.L., Simpson, G.B., and Treiman, R. (2007). The English Lexicon Project. Behav. Res. Methods *39*, 445–459.

Barch, D.M., Burgess, G.C., Harms, M.P., Petersen, S.E., Schlaggar, B.L., Corbetta, M., Glasser, M.F., Curtiss, S., Dixit, S., Feldt, C., et al.; WU-Minn HCP Consortium (2013). Function in the human connectome: task-fMRI and individual differences in behavior. Neuroimage *80*, 169–189.

Barton, R.A., and Venditti, C. (2014). Rapid evolution of the cerebellum in humans and other great apes. Curr. Biol. *24*, 2440–2444.

Behzadi, Y., Restom, K., Liau, J., and Liu, T.T. (2007). A component based noise correction method (CompCor) for BOLD and perfusion based fMRI. Neuroimage *37*, 90–101.

Braga, R.M., and Buckner, R.L. (2017). Parallel Interdigitated Distributed Networks within the Individual Estimated by Intrinsic Functional Connectivity. Neuron *95*, 457–471.e5.

Buckner, R.L. (2013). The cerebellum and cognitive function: 25 years of insight from anatomy and neuroimaging. Neuron *80*, 807–815.

Buckner, R.L., Krienen, F.M., Castellanos, A., Diaz, J.C., and Yeo, B.T. (2011). The organization of the human cerebellum estimated by intrinsic functional connectivity. J. Neurophysiol. *106*, 2322–2345.

Caligiore, D., Pezzulo, G., Baldassarre, G., Bostan, A.C., Strick, P.L., Doya, K., Helmich, R.C., Dirkx, M., Houk, J., Jörntell, H., et al. (2017). Consensus paper: towards a systems-level view of cerebellar function: the interplay between cerebellum, basal ganglia, and cortex. Cerebellum *16*, 203–229.

Carp, J. (2013). Optimizing the order of operations for movement scrubbing: Comment on Power et al. Neuroimage *76*, 436–438.

Chen, Y.L., Tu, P.C., Lee, Y.C., Chen, Y.S., Li, C.T., and Su, T.P. (2013). Resting-state fMRI mapping of cerebellar functional dysconnections involving multiple large-scale networks in patients with schizophrenia. Schizophr. Res. *149*, 26–34.

Chen, C.H., Fremont, R., Arteaga-Bracho, E.E., and Khodakhah, K. (2014). Short latency cerebellar modulation of the basal ganglia. Nat. Neurosci. *17*, 1767–1775.

Choi, E.Y., Yeo, B.T., and Buckner, R.L. (2012). The organization of the human striatum estimated by intrinsic functional connectivity. J. Neurophysiol. *108*, 2242–2263.

Ciric, R., Wolf, D.H., Power, J.D., Roalf, D.R., Baum, G.L., Ruparel, K., Shinohara, R.T., Elliott, M.A., Eickhoff, S.B., Davatzikos, C., et al. (2017). Benchmarking of participant-level confound regression strategies for the control of motion artifact in studies of functional connectivity. Neuroimage *154*, 174–187.

Connor, L.T., DeShazo Braby, T., Snyder, A.Z., Lewis, C., Blasi, V., and Corbetta, M. (2006). Cerebellar activity switches hemispheres with cerebral recovery in aphasia. Neuropsychologia *44*, 171–177.

Dale, A.M., Fischl, B., and Sereno, M.I. (1999). Cortical surface-based analysis. I. Segmentation and surface reconstruction. Neuroimage *9*, 179–194.

Diedrichsen, J., and Zotow, E. (2015). Surface-based display of volume-averaged cerebellar imaging data. PLoS ONE *10*, e0133402.

Dosenbach, N.U., Visscher, K.M., Palmer, E.D., Miezin, F.M., Wenger, K.K., Kang, H.C., Burgund, E.D., Grimes, A.L., Schlaggar, B.L., and Petersen, S.E. (2006). A core system for the implementation of task sets. Neuron *50*, 799–812.

Dosenbach, N.U., Fair, D.A., Miezin, F.M., Cohen, A.L., Wenger, K.K., Dosenbach, R.A., Fox, M.D., Snyder, A.Z., Vincent, J.L., Raichle, M.E., et al. (2007). Distinct brain networks for adaptive and stable task control in humans. Proc. Natl. Acad. Sci. USA *104*, 11073–11078.

Dum, R.P., and Strick, P.L. (2003). An unfolded map of the cerebellar dentate nucleus and its projections to the cerebral cortex. J. Neurophysiol. *89*, 634–639.

Fiez, J.A. (1996). Cerebellar contributions to cognition. Neuron *16*, 13–15.

Fiez, J.A., Petersen, S.E., Cheney, M.K., and Raichle, M.E. (1992). Impaired non-motor learning and error detection associated with cerebellar damage. A single case study. Brain *115*, 155–178.

Fischl, B. (2012). FreeSurfer. Neuroimage *62*, 774–781.

Fischl, B., Sereno, M.I., and Dale, A.M. (1999). Cortical surface-based analysis. II: Inflation, flattening, and a surface-based coordinate system. Neuroimage *9*, 195–207.

Fries, P. (2015). Rhythms for cognition: communication through coherence. Neuron *88*, 220–235.

Gardner, R.J., Coleman, L.T., Mitchell, L.A., Smith, L.J., Harvey, A.S., Scheffer, I.E., Storey, E., Nowotny, M.J., Sloane, R.A., and Lubitz, L. (2001). Near-total absence of the cerebellum. Neuropediatrics *32*, 62–68.

Glasser, M.F., Sotiropoulos, S.N., Wilson, J.A., Coalson, T.S., Fischl, B., Andersson, J.L., Xu, J., Jbabdi, S., Webster, M., Polimeni, J.R., et al.; WU-Minn HCP Consortium (2013). The minimal preprocessing pipelines for the Human Connectome Project. Neuroimage *80*, 105–124.

Glasser, M.F., Coalson, T.S., Robinson, E.C., Hacker, C.D., Harwell, J., Yacoub, E., Ugurbil, K., Andersson, J., Beckmann, C.F., Jenkinson, M., et al. (2016). A multi-modal parcellation of human cerebral cortex. Nature *536*, 171–178.

Gordon, E.M., Laumann, T.O., Adeyemo, B., Huckins, J.F., Kelley, W.M., and Petersen, S.E. (2016). Generation and evaluation of a cortical area parcellation from resting-state correlations. Cereb. Cortex *26*, 288–303.

Gordon, E.M., Laumann, T.O., Adeyemo, B., Gilmore, A.W., Nelson, S.M., Dosenbach, N.U.F., and Petersen, S.E. (2017a). Individual-specific features of brain systems identified with resting state functional correlations. Neuroimage *146*, 918–939.

Gordon, E.M., Laumann, T.O., Adeyemo, B., and Petersen, S.E. (2017b). Individual variability of the system-level organization of the human brain. Cereb. Cortex *27*, 386–399.

Gordon, E.M., Laumann, T.O., Gilmore, A.W., Newbold, D.J., Greene, D.J., Berg, J.J., Ortega, M., Hoyt-Drazen, C., Gratton, C., Sun, H., et al. (2017c). Precision functional mapping of individual human brains. Neuron *95*, 791–807.e7.

Gratton, C., Laumann, T.O., Nielsen, A.N., Greene, D.J., Gordon, E.M., Gilmore, A.W., Nelson, S.M., Coalson, R.S., Snyder, A.Z., Schlaggar, B.L., et al. (2018). Functional brain networks are dominated by stable group and individual factors, not cognitive or daily variation. Neuron *98*, 439–452.e5.

Grayson, D.S., and Fair, D.A. (2017). Development of large-scale functional networks from birth to adulthood: A guide to the neuroimaging literature. Neuroimage *160*, 15–31.

Greene, D.J., Laumann, T.O., Dubis, J.W., Ihnen, S.K., Neta, M., Power, J.D., Pruett, J.R., Jr., Black, K.J., and Schlaggar, B.L. (2014). Developmental changes in the organization of functional connections between the basal ganglia and cerebral cortex. J. Neurosci. *34*, 5842–5854.

Greene, D.J., Church, J.A., Dosenbach, N.U., Nielsen, A.N., Adeyemo, B., Nardos, B., Petersen, S.E., Black, K.J., and Schlaggar, B.L. (2016). Multivariate pattern classification of pediatric Tourette syndrome using functional connectivity MRI. Dev. Sci. *19*, 581–598.

Hallquist, M.N., Hwang, K., and Luna, B. (2013). The nuisance of nuisance regression: spectral misspecification in a common approach to resting-state fMRI preprocessing reintroduces noise and obscures functional connectivity. Neuroimage *82*, 208–225.

Hwang, K., Bertolero, M.A., Liu, W.B., and D'Esposito, M. (2017). The human thalamus is an integrative hub for functional brain networks. J. Neurosci. *37*, 5594–5607.

Kelly, R.M., and Strick, P.L. (2003). Cerebellar loops with motor cortex and prefrontal cortex of a nonhuman primate. J. Neurosci. *23*, 8432–8444.

Krienen, F.M., and Buckner, R.L. (2009). Segregated fronto-cerebellar circuits revealed by intrinsic functional connectivity. Cereb. Cortex *19*, 2485–2497.

Laumann, T.O., Gordon, E.M., Adeyemo, B., Snyder, A.Z., Joo, S.J., Chen, M.Y., Gilmore, A.W., McDermott, K.B., Nelson, S.M., Dosenbach, N.U., et al. (2015). Functional system and areal organization of a highly sampled individual human brain. Neuron *87*, 657–670.

Leiner, H.C., Leiner, A.L., and Dow, R.S. (1989). Reappraising the cerebellum: what does the hindbrain contribute to the forebrain? Behav. Neurosci. *103*, 998–1008.

Luna, B., Marek, S., Larsen, B., Tervo-Clemmens, B., and Chahal, R. (2015). An integrative model of the maturation of cognitive control. Annu. Rev. Neurosci. *38*, 151–170.

Manns, I.D., Sakmann, B., and Brecht, M. (2004). Sub- and suprathreshold receptive field properties of pyramidal neurones in layers 5A and 5B of rat somatosensory barrel cortex. J. Physiol. *556*, 601–622.

Marcus, D.S., Harwell, J., Olsen, T., Hodge, M., Glasser, M.F., Prior, F., Jenkinson, M., Laumann, T., Curtiss, S.W., and Van Essen, D.C. (2011). Informatics and data mining tools and strategies for the human connectome project. Front. Neuroinform. *5*, 4.

Marek, S., and Dosenbach, N.U.F. (2018). The frontoparietal network: function, electrophysiology, and importance of individual precision mapping. Dialogues Clin. Neurosci. *20*, 133–140.

Marek, S., Hwang, K., Foran, W., Hallquist, M.N., and Luna, B. (2015). The contribution of network organization and integration to the development of cognitive control. PLoS Biol. *13*, e1002328.

Marko, M.K., Crocetti, D., Hulst, T., Donchin, O., Shadmehr, R., and Mostofsky, S.H. (2015). Behavioural and neural basis of anomalous motor learning in children with autism. Brain *138*, 784–797.

Mitra, A., Snyder, A.Z., Hacker, C.D., and Raichle, M.E. (2014). Lag structure in resting-state fMRI. J. Neurophysiol. *111*, 2374–2391.

Mitra, A., Snyder, A.Z., Blazey, T., and Raichle, M.E. (2015). Lag threads organize the brain's intrinsic activity. Proc. Natl. Acad. Sci. USA *112*, E2235–E2244.

Mitra, A., Snyder, A.Z., Hacker, C.D., Pahwa, M., Tagliazucchi, E., Laufs, H., Leuthardt, E.C., and Raichle, M.E. (2016). Human cortical-hippocampal dialogue in wake and slow-wave sleep. Proc. Natl. Acad. Sci. USA *113*, E6868–E6876.

Mitra, A., Kraft, A., Wright, P., Acland, B., Snyder, A.Z., Rosenthal, Z., Czerniewski, L., Bauer, A., Snyder, L., Culver, J., et al. (2018). Spontaneous infra-slow brain activity has unique spatiotemporal dynamics and laminar structure. Neuron *98*, 297–305.e6.

Monsell, S. (2003). Task switching. Trends Cogn. Sci. *7*, 134–140.

O'Reilly, J.X., Beckmann, C.F., Tomassini, V., Ramnani, N., and Johansen-Berg, H. (2010). Distinct and overlapping functional zones in the cerebellum defined by resting state functional connectivity. Cereb. Cortex *20*, 953–965.

Oelschlager, H.H.A. (2000). Morphological and functional adaptations of the toothed whale head in aquatic life. Hist. Biol. *14*, 33–39.

Parker, K.L., Kim, Y.C., Kelley, R.M., Nessler, A.J., Chen, K.H., Muller-Ewald, V.A., Andreasen, N.C., and Narayanan, N.S. (2017). Delta-frequency stimulation of cerebellar projections can compensate for schizophrenia-related medial frontal dysfunction. Mol. Psychiatry *22*, 647–655.

Petersen, S.E., Fox, P.T., Posner, M.I., Mintun, M., and Raichle, M.E. (1989). Positron emission tomographic studies of the processing of singe words. J. Cogn. Neurosci. *1*, 153–170.

Popa, T., Velayudhan, B., Hubsch, C., Pradeep, S., Roze, E., Vidailhet, M., Meunier, S., and Kishore, A. (2013). Cerebellar processing of sensory inputs primes motor cortex plasticity. Cereb. Cortex *23*, 305–314.

Power, J.D., Cohen, A.L., Nelson, S.M., Wig, G.S., Barnes, K.A., Church, J.A., Vogel, A.C., Laumann, T.O., Miezin, F.M., Schlaggar, B.L., and Petersen, S.E. (2011). Functional network organization of the human brain. Neuron *72*, 665–678.

Power, J.D., Barnes, K.A., Snyder, A.Z., Schlaggar, B.L., and Petersen, S.E. (2013). Steps toward optimizing motion artifact removal in functional connectivity MRI; a reply to Carp. Neuroimage *76*, 439–441.

Power, J.D., Mitra, A., Laumann, T.O., Snyder, A.Z., Schlaggar, B.L., and Petersen, S.E. (2014). Methods to detect, characterize, and remove motion artifact in resting state fMRI. Neuroimage *84*, 320–341.

Power, J.D., Schlaggar, B.L., and Petersen, S.E. (2015). Recent progress and outstanding issues in motion correction in resting state fMRI. Neuroimage *105*, 536–551.

Raz, N., Schmiedek, F., Rodrigue, K.M., Kennedy, K.M., Lindenberger, U., and Lövdén, M. (2013). Differential brain shrinkage over 6 months shows limited association with cognitive practice. Brain Cogn. *82*, 171–180.

Righi, G., Peissig, J.J., and Tarr, M.J. (2012). Recognizing disguised faces. Vis. Cogn. *20*, 143–169.

Robinson, E.C., Jbabdi, S., Glasser, M.F., Andersson, J., Burgess, G.C., Harms, M.P., Smith, S.M., Van Essen, D.C., and Jenkinson, M. (2014). MSM: a new flexible framework for Multimodal Surface Matching. Neuroimage *100*, 414–426.

Rosvall, M., and Bergstrom, C.T. (2008). Maps of random walks on complex networks reveal community structure. Proc. Natl. Acad. Sci. USA *105*, 1118–1123.

Sami, S., Robertson, E.M., and Miall, R.C. (2014). The time course of task-specific memory consolidation effects in resting state networks. J. Neurosci. *34*, 3982–3992.

Satterthwaite, T.D., Elliott, M.A., Gerraty, R.T., Ruparel, K., Loughead, J., Calkins, M.E., Eickhoff, S.B., Hakonarson, H., Gur, R.C., Gur, R.E., and Wolf, D.H. (2013). An improved framework for confound regression and filtering for control of motion artifact in the preprocessing of resting-state functional connectivity data. Neuroimage *64*, 240–256.

Schmahmann, J.D. (2004). Disorders of the cerebellum: ataxia, dysmetria of thought, and the cerebellar cognitive affective syndrome. J. Neuropsychiatry Clin. Neurosci. *16*, 367–378.

Schmahmann, J.D., and Sherman, J.C. (1998). The cerebellar cognitive affective syndrome. Brain *121*, 561–579.

Schmahmann, J.D., Macmore, J., and Vangel, M. (2009). Cerebellar stroke without motor deficit: clinical evidence for motor and non-motor domains within the human cerebellum. Neuroscience *162*, 852–861.

Smith, S.M., Jenkinson, M., Woolrich, M.W., Beckmann, C.F., Behrens, T.E., Johansen-Berg, H., Bannister, P.R., De Luca, M., Drobnjak, I., Flitney, D.E., et al. (2004). Advances in functional and structural MR image analysis and implementation as FSL. Neuroimage *23* (*Suppl 1*), S208–S219.

Stoet, G., and Snyder, L.H. (2003). Executive control and task-switching in monkeys. Neuropsychologia *41*, 1357–1364.

Strick, P.L., Dum, R.P., and Fiez, J.A. (2009). Cerebellum and nonmotor function. Annu. Rev. Neurosci. *32*, 413–434.

Talairach, J., and Tournoux, P. (1988). Co-planar stereotaxic atlas of the human brain (New York: Thieme Medical Publishers, Inc).

Thach, W.T. (2007). On the mechanism of cerebellar contributions to cognition. Cerebellum *6*, 163–167.

Tomasi, D., and Volkow, N.D. (2012). Abnormal functional connectivity in children with attention-deficit/hyperactivity disorder. Biol. Psychiatry *71*, 443–450.

Vaishnavi, S.N., Vlassenko, A.G., Rundle, M.M., Snyder, A.Z., Mintun, M.A., and Raichle, M.E. (2010). Regional aerobic glycolysis in the human brain. Proc. Natl. Acad. Sci. USA *107*, 17757–17762.

Van Essen, D.C., Glasser, M.F., Dierker, D.L., Harwell, J., and Coalson, T. (2012). Parcellations and hemispheric asymmetries of human cerebral cortex analyzed on surface-based atlases. Cereb. Cortex *22*, 2241–2262.

van Kerkoerle, T., Self, M.W., Dagnino, B., Gariel-Mathis, M.A., Poort, J., van der Togt, C., and Roelfsema, P.R. (2014). Alpha and gamma oscillations characterize feedback and feedforward processing in monkey visual cortex. Proc. Natl. Acad. Sci. USA *111*, 14332–14341.

Yarkoni, T., Poldrack, R.A., Nichols, T.E., Van Essen, D.C., and Wager, T.D. (2011). Large-scale automated synthesis of human functional neuroimaging data. Nat. Methods *8*, 665–670.

Yeo, B.T., Krienen, F.M., Sepulcre, J., Sabuncu, M.R., Lashkari, D., Hollinshead, M., Roffman, J.L., Smoller, J.W., Zöllei, L., Polimeni, J.R., et al. (2011). The organization of the human cerebral cortex estimated by intrinsic functional connectivity. J. Neurophysiol. *106*, 1125–1165.

# STAR★METHODS

## KEY RESOURCES TABLE

| REAGENT or RESOURCE | SOURCE | IDENTIFIER |
|---|---|---|
| Deposited Data | | |
| Raw and processed MRI data | (Gordon et al., 2017c) | https://openneuro.org/datasets/ds000224; Accession # ds000224 |
| Task fMRI activations | (Gordon et al., 2017c) | https://neurovault.org/collections/2447/ |
| Psychological Image Collection at Stirling 2D face set | N/A | http://pics.psych.stir.ac.uk/ |
| CNBC Tarrlab "Face Place" repository | (Righi et al., 2012) | http://wiki.cnbc.cmu.edu/Face_Place |
| Park Aging Mind Laboratory Face Database | N/A | http://agingmind.utdallas.edu/download-stimuli/face-database/ |
| Libor Spacek's Facial Imaging Database | N/A | http://cmp.felk.cvut.cz/~spacelib/faces/ |
| English Lexicon Project | (Balota et al., 2007) | http://elexicon.wustl.edu/ |
| Software and Algorithms | | |
| MATLAB | MathWorks | RRID: SCR_001622; https://www.mathworks.com/ |
| Connectome Workbench | (Marcus et al., 2011) | RRID: SCR_008750; https://www.humanconnectome.org/software/connectome-workbench |
| Freesurfer | (Dale et al., 1999) | RRID: SCR_001847; https://surfer.nmr.mgh.harvard.edu/ |
| FSL | (Smith et al., 2004) | RRID: SCR_002823; https://fsl.fmrib.ox.ac.uk/fsl/fslwiki |
| 4dfp tools | N/A | ftp://imaging.wustl.edu/pub/raichlab/4dfp_tools/ |
| Freesurfer to fs_LR pipeline | (Van Essen et al., 2012) | http://brainvis.wustl.edu |
| Parcellation code | (Gordon et al., 2016) | https://sites.wustl.edu/petersenschlaggarlab/resources/ |
| Infomap | (Rosvall and Bergstrom, 2008) | http://www.mapequation.org/ |

## CONTACT FOR REAGENT AND RESOURCE SHARING

Further information and requests for resources should be directed to and will be fulfilled by the Lead Contact, Scott Marek (smarek@wustl.edu).

## EXPERIMENTAL MODEL AND SUBJECT DETAILS

The publicly available Midnight Scan Club (MSC) dataset was used for analyses (https://openneuro.org/datasets/ds000224). The dataset and processing has been previously described in detail (Gordon et al., 2017c). Below we detail minor modifications in the processing of the data, namely multimodal surface mapping and the handling of white matter and CSF regressors. We then describe specific analyses employed in this manuscript.

### Participants and Study Design

The MSC dataset includes structural and functional MRI data, as well as behavioral measures from 10 individuals (5 females, ages 24-34) scanned in 10 different sessions. Each session occurred on a separate day, beginning at midnight. Daily sessions were conducted in close succession, with all sessions completed within 7 weeks for all participants. provided written informed consent. Procedures were approved by the Washington University Institutional Review Board and School of Medicine Human Studies Committee. During each of the scanning sessions, participants completed a resting-state scan followed by fMRI scans in four other task states: a motor task, a semantic task, a coherence task, and an incidental encoding memory task. MRI acquisition parameters and tasks are described below.

## METHOD DETAILS

### MRI image acquisition

Imaging for each subject was performed on a Siemens TRIO 3T MRI scanner over the course of 12 sessions conducted on separate days, each beginning at midnight. Structural MRI was conducted across two separate days. In total, four T1-weighted images

(sagittal, 224 slices, 0.8 mm isotropic resolution, TE = 3.74 ms, TR = 2400 ms, TI = 1000 ms, flip angle = 8 degrees), four T2-weighted images (sagittal, 224 slices, 0.8 mm isotropic resolution, TE = 479 ms, TR = 3200 ms), four MRA (transverse, 0.6 × 0.6, x 1.0mm, 44 slices, TR = 25ms, TE = 3.34ms) and eight MRVs, including four in coronal and four in sagittal orientations (sagittal: 0.8 × 0.8 × 2.0mm thickness, 120 slices, TR = 27ms, TE = 7.05ms; coronal: 0.7 × 0.7 × 2.5mm thickness, 128 slices, TR = 28ms TE = 7.18ms), were obtained for each subject. Analyses of the MRA and MRV scans are not reported here.

On ten subsequent days, each subject underwent 1.5 hour functional MRI scanning beginning at midnight. In each session, we first collected thirty contiguous minutes of resting state fMRI data, in which subjects visually fixated on a white crosshair presented against a black background. Each subject was then scanned during performance of three separate tasks: motor (2 runs per session, 7.8 min combined), incidental memory (3 runs per session, 13.1 min combined), mixed design (2 runs per session, 14.2 min combined). Data from the incidental memory task and mixed design is not included in the current work. Across all sessions, each subject was scanned for 300 total minutes during the resting state and approximately 350 total minutes during task performance. All functional imaging was performed using a gradient-echo EPI sequence (TR = 2.2 s, TE = 27 ms, flip angle = 90°, voxel size = 4 mm x 4 mm x 4 mm, 36 slices). In each session, one gradient echo field map sequence was acquired with the same prescription as the functional images. An EyeLink 1000 eye-tracking system (https://www.sr-research.com) allowed continuous monitoring of subjects' eyes in order to check for periods of prolonged eye closure, potentially indicating sleep. Only one subject (MSC08) demonstrated prolonged eye closures.

### Motor task design

The motor task was adapted from that used in the Human Connectome Project (Barch et al., 2013). Subjects were presented with visual cues that directed them to close and relax their hands, flex and relax their toes, or wiggle their tongue. Each block started with a 2.2 s cue indicating which movement was to be made. After this cue, a centrally-presented caret replaced the instruction and flickered once every 1.1 s (without temporal jittering). Each time the caret flickered, subjects executed the proper movement. Twelve movements were made per block. Each task run consisted of 2 blocks of each type of movement as well as 3 blocks of resting fixation, which lasted 15.4 s.

### Cortical surface generation

Generation of cortical surfaces from the MRI data followed a procedure similar to that previously described in (Laumann et al., 2015). First, anatomical surfaces were generated from the subject's average T1-weighted image in native volumetric space using FreeSurfer's default recon-all processing pipeline (version 5.3). This pipeline first conducted brain extraction and segmentation. After this step, segmentations were hand-edited to maximize accuracy. Subsequently, the remainder of the recon-all pipeline was conducted on the hand-edited segmentations, including generation of white matter and pial surfaces, inflation of the surfaces to a sphere, and surface shape-based spherical registration of the subject's original surface to the fsaverage surface (Dale et al., 1999; Fischl et al., 1999). The fsaverage-registered left and right hemisphere surfaces were brought into register with each other using deformation maps from a landmark-based registration of left and right fsaverage surfaces to a hybrid left-right fsaverage surface ('fs_LR'). These fs_LR spherical template meshes were input to a flexible Multi-modal surface Matching (MSM) algorithm using sulc features to register templates to the atlas mesh (Robinson et al., 2014). These newly registered surfaces were then down-sampled to a 32,492 vertex surface (fs_LR 32k) for each hemisphere. The various structural metric data (thickness,curv,etc..) from the original surfaces to the fs_LR 32k surface were composed into a single deformation map allowing for one step resampling. MSM registration provided a more optimal fit of pial and white surfaces and reduced areal distortion (Glasser et al., 2016). These various surfaces in native stereotaxic space were then transformed into atlas space (711-2B) by applying the previously calculated T1-to-atlas transformation.

### fMRI Preprocessing

Functional data were preprocessed to reduce artifact and to maximize cross-session registration. All sessions underwent correction of odd versus even slice intensity differences attributable to interleaved acquisition, intensity normalization to a whole brain mode value of 1000, and within run correction for head movement. Atlas transformation was computed by registering the mean intensity image from a single BOLD session to Talairach atlas space (Talairach and Tournoux, 1988) via the average high-resolution T2-weighted image and average high-resolution T1-weighted image. All subsequent BOLD sessions were linearly registered to this first session. This atlas transformation, mean field distortion correction (see below), and resampling to 3-mm isotropic atlas space were combined into a single interpolation using FSL's applywarp tool. Unless otherwise specified, all subsequent operations were performed on the atlas-transformed volumetric time series. In some instances, we compare our main results with voxel-wise analyses (across both cortex and cerebellum) after non-linearly transforming all subjects to a reference subject (MSC 01). For methodological details of this procedure, see below (Non-linear registration of volumetric time series).

### Distortion correction

A mean field map was generated based on the field maps collected in each subject (Laumann et al., 2015). This mean field map was then applied to all sessions for distortion correction. To generate the mean field map the following procedure was used: (1) Field map magnitude images were mutually co-registered. (2) Transforms between all sessions were resolved. Transform resolution reconstructs the n-1 transforms between all images using the n(n-1)/2 computed transform pairs. (3) The resolved transforms were applied

to generate a mean magnitude image. (4) The mean magnitude image was registered to an atlas representative template. (5) Individual session magnitude image to atlas space transforms were computed by composing the session-to-mean and mean-to-atlas transforms. (6) Phase images were then transformed to atlas space using the composed transforms, and a mean phase image in atlas space was computed.

Application of mean field map to individual fMRI sessions: (1) For each session, field map uncorrected data was registered to atlas space, as above. (2) The generated transformation matrix was then inverted and applied to the mean field map to bring the mean field map into the session space. (3) The mean field map was used to correct distortion in each native-space run of resting state and task data in the session. (4) The undistorted data was then re-registered to atlas space. (5) This new transformation matrix and the mean field map then were applied together to resample each run of resting state and task data in the session to undistorted atlas space in a single step.

### RSFC Preprocessing

Additional preprocessing steps to reduce spurious variance unlikely to reflect neuronal activity were executed as recommended in Ciric et al. (2017) and Power et al. (2014). First, temporal masks were created to flag motion-contaminated frames. We observed that two subjects (MSC 03 and MSC 10) had a high-frequency artifact in the motion estimates calculated in the phase encode (anterior-posterior) direction that did not appear to reflect biological movement. We thus filtered the motion estimate time courses in this direction only to retain effects occurring below 0.1 Hz in all subjects for consistency. Motion contaminated volumes were then identified by frame-by-frame displacement (FD). Frames with FD > 0.2mm were flagged as motion-contaminated and > 0.5mm in the lag analysis to retain larger contiguous chunks of data. Across all subjects, these masks censored 28% ± 18% (range: 6% – 67%) of the data; on average, subjects retained 5929 ± 1508 volumes (range: 2733 – 7667). Note that in this paradigm, even the worst subject retained almost two hours of data.

After computing the temporal masks for high motion frame censoring, the data were processed with the following steps: (i) demeaning and detrending, (ii) interpolation across censored frames using least-squares spectral estimation of the values at censored frames (Power et al., 2014) so that continuous data can be passed through (iii) a band-pass filter (0.005 Hz < f < 0.10 Hz) without re-introducing nuisance signals (Hallquist et al., 2013) or contaminating frames near high motion frames (Carp, 2013; Power et al., 2013) and (iv), multiple regression including: whole brain, principle components of ventricular and white matter signals (see below Component-based nuisance regression), and motion regressors derived by Volterra expansion, with censored data ignored during beta estimation, and (v) upsampling to 2mm isotropic voxels. Censored frames were then excised from the data for all subsequent analyses.

### Component-based nuisance regression

Next, the filtered BOLD time series underwent a component-based nuisance regression approach incorporating elements of previously published methods (Behzadi et al., 2007). Nuisance regression using time series extracted from white matter and cerebrospinal fluid (CSF) assumes that variance in such regions is unlikely to reflect neural activity. Variance in these regions is known to correspond largely to physiological noise (e.g., CSF pulsations), arterial $pCO_2$-dependent changes in T2*-weighted intensity and motion artifact; this spurious variance is widely shared with regions of interest in gray matter. We also included the mean signal averaged over the whole brain as a nuisance regressor. Global signal regression (GSR) has been controversial. However, the available evidence indicates that GSR is a highly effective de-noising strategy (Ciric et al., 2017; Power et al., 2015).

Nuisance regressors were extracted from white matter and ventricle masks, first segmented by FreeSurfer (Fischl, 2012), then spatially resampled in register with the fMRI data. Voxels surrounding the edge of the brain are particularly susceptible to motion artifacts and CSF pulsations (Satterthwaite et al., 2013); hence, a third nuisance mask was created for the extra-axial compartment by thresholding the temporal standard deviation image (SDt > 2.5%), excluding a dilated whole brain mask. Voxel-wise nuisance time series were dimensionality reduced as in CompCor (Behzadi et al., 2007), except that the number of retained regressors, rather than being a fixed quantity, was determined, for each noise compartment, by orthogonalization of the covariance matrix and retaining components ordered by decreasing eigenvalue up to a condition number of 30 $(\lambda_{max}/\lambda_{min} > 30)$. The retained components across all compartments formed the columns of a design matrix, $X$, along with the global signal, its first derivative, and the six time series derived by retrospective motion correction. The columns of $X$ are likely to exhibit substantial co-linearity. Therefore, to prevent numerical instability owing to rank-deficiency during nuisance regression, a second-level SVD was applied to $XX^T$ to impose an upper limit of 250 on the condition number. This final set of regressors was applied in a single step to the filtered, interpolated BOLD time series.

### Surface processing and CIFTI generation of BOLD data

Surface processing of the RSFC BOLD data proceeded through the following steps. First, the BOLD fMRI volumetric timeseries (both resting-state and task) are sampled to each subject's original mid-thickness left and right-hemisphere surfaces (generated as the average of the white and pial surfaces) using the ribbon-constrained sampling procedure available in Connectome Workbench 1.0. This procedure samples data from voxels within the gray matter ribbon (i.e., between the white and pial surfaces) that lie in a cylinder orthogonal to the local mid-thickness surface weighted by the extent to which the voxel falls within the ribbon. Voxels with a timeseries coefficient of variation 0.5 standard deviations higher than the mean coefficient of variation of nearby voxels (within

a 5 mm sigma Gaussian neighborhood) were excluded from the volume to surface sampling, as described in Glasser et al. (2013). Once sampled to the surface, time courses were deformed and resampled from the individual's original surface to the 32k fs_LR surface in a single step using the deformation map generated above (in "Cortical surface generation"). This resampling allows point-to-point comparison between each individual registered to this surface space.

These surfaces were then combined with volumetric subcortical and cerebellar data into the CIFTI format using Connectome Workbench (Marcus et al., 2011), creating full brain time courses excluding non-gray matter tissue. Subcortical (including accumbens, amygdala, caudate, hippocampus, pallidum, putamen, and thalamus) and cerebellar voxels were selected based on the FreeSurfer segmentation of the individual subject's native-space average T1, transformed into atlas space, and manually inspected. Finally, the resting-state time courses were smoothed with geodesic 2D (for surface data) and Euclidean 3D (for volumetric data) Gaussian kernels ($\sigma$ = 2.55 mm).

### Vertex-wise network mapping

The network organization of each subject's cortical surface was derived using the graph-theory-based Infomap algorithm for community detection (Rosvall and Bergstrom, 2008), following Power et al. (2011). In this approach, we calculated the Pearson correlation matrix of the time courses from all cortical vertices, concatenated across sessions. Correlations between vertices within 30 mm of each other were set to zero. Geodesic distance was used for within-hemisphere surface connections. Inter-hemispheric connections between the cortical surfaces were retained, as smoothing was not performed across the mid-sagittal plane.

This matrix was then thresholded at a range of values calculated based on the resulting density of the matrix; the density thresholds ranged from 0.1% to 5%. Small networks with 400 or fewer vertices / voxels were considered unassigned and removed from further consideration as in Gordon et al. (2017c). The above analysis was conducted in each individual subject, and in data averaged across all subjects (MSC Average).

To identify putative networks we may find in each subject, we conducted a re-analysis of our previous work on group-average data (Gordon et al., 2017b), in which the Infomap algorithm was conducted in data averaged across a large, independent group of 120 individuals with low quantities of per-subject data. Analysis procedures were identical to the analyses conducted on this group in Gordon et al. (2017b), except that the minimum density threshold tested was reduced to 0.1%. As a result, we were able to identify group-average networks corresponding to a) early visual cortex, b) somatomotor cortex associated with the foot, and c) to a strip along postcentral gyrus corresponding closely to "pre-motor" activation in the Neurosynth platform (Yarkoni et al., 2011).

Putative network identities were then assigned to each subject's communities similar to previously published work from our group (see Gordon et al., 2017c). Figure S3 contains individual and group averaged Infomap community assignments on the cortical surface.

### Regression of adjacent cortical tissue

The most dorsal regions of the cerebellum are in close anatomical proximity to the ventral portions of the occipital lobes, resulting in spurious functional coupling between ventral visual voxels and dorsal cerebellar voxels. To reduce this artifact, we regressed the cortical signal within 20mm of a given cerebellar voxel, for each cerebellar voxel (Buckner et al., 2011). More specifically, we used Euclidean distance as our metric between cerebellar voxels and cortical surface vertices. The BOLD time series from all vertices falling within 20mm of a source voxel were averaged and then regressed from the cerebellar voxel time series. The resulting residual timeseries were used for all subsequent analyses.

### Winner-take-all parcellation of the cerebellum

The network organization of each subject's cerebellum was assigned using a winner-take-all approach (Buckner et al., 2011; Choi et al., 2012; Greene et al., 2014; Hwang et al., 2017). For each subject, we concatenated the time series of BOLD activity across the 10 scanning sessions across the whole brain, using the residual time series of each cerebellar voxel computed above. After excluding high motion frames, we correlated each cortical vertex and cerebellar voxel with every other vertex and voxel, resulting in a whole brain correlation matrix. Next, for each cerebellar voxel we computed the average correlation between a given voxel and vertices within each cortical network in the contralateral hemisphere, resulting in a single correlation value between a voxel and each cortical network. The network affiliation of a given voxel was assigned to the network to which it had the greatest positive correlation. All non-zero correlations (both positive and negative) were included in the analysis. Supplemental figures of WTA and subsequent results displayed on cerebellar flat maps were generated using the SUIT toolbox (Diedrichsen and Zotow, 2015).

### RSFC and WTA reliability

Individual subject RSFC reliability and was assessed in each subject using an iterative comparison of random data subsets, similar to Gordon et al. (2017c) and Laumann et al. (2015). For each subject, the ten scanning sessions were split into two equal-sized, randomly selected subsets of sessions. One half of (post-motion censoring) data was randomly selected from one of the two subsets to use as the comparison set of data. A varying amount of data (ranging in 5 min intervals from 5 min to 100 min, when possible) was randomly selected from the other subset. Whereas Gordon et al. (2017c) and Laumann et al. (2015) calculated split-half reliability using individual parcels, determined reliability at the vertex/voxel x network level to maximize comparability between the cerebellum and cortex. Thus, in both the comparison and test set, we averaged the time series of activity within each individual subject's

Infomap-derived cortical functional network and subsequently correlated the time series of every vertex/voxel with each network. To determine reliability, we then calculated the average correlation between the test and comparison set of data.

Cerebellum WTA reliability was calculated similarly, by first repeating the same procedure to split the data into a test and comparison set. We repeated the WTA procedure to partition the cerebellum in functional networks in the comparison set and for each test set. Iterative split-half reliability was determined by calculating the Spearman correlation between WTA assignments in the test and comparison dataset.

### Network specificity

To assess the specificity of cerebellar network assignments, we took two approaches. First, for each cerebellar voxel, we calculated the percent difference in correlation between the average correlation to the 'winning' cortical network and to the 2$^{nd}$ place network. Cerebellar voxels with greater difference in mean correlation between 1$^{st}$ and 2$^{nd}$ place cortical networks represent areas of high network specificity.

### Task/Rest Convergence

For each task condition (right hand, left hand, right foot, left foot or tongue movement), a 35.2 s time course was extracted from every image voxel starting with each stimulus presentation. These time courses included the 15.4 s movement block and an additional 19.8 s to capture a full hemodynamic response. Then, for each voxel, time courses from all task trials were correlated against one another. Pairwise correlations between trials were averaged together to produce one value per voxel. This yields very low correlation values at voxels showing inconsistent (i.e., uncorrelated) time courses from one trial to another, but is sensitive to any voxel showing a consistent activation time course across trials.

To determine task/rest convergence within the cerebellum, for each motor subdivision, we correlated the resting state BOLD signal from the cortical vertex demonstrating peak correlated activity from the task analysis and thresholded the resulting cerebellar voxel-wise correlations at 0.10 for foot and 0.15 for both hand and face motor subdivisions. This same threshold was applied to the task data in the cerebellum. We defined convergence as voxels in the cerebellum demonstrating suprathreshold correlations for both task and rest and super imposed this patch over the WTA network partitions.

### Network Similarity: Group level versus individual level effects

A detailed account of methods for this analysis can be found in Gratton et al. (2018). We provide an overview of aspects of those analyses pertinent to this study. Group versus individual level effects were examined by creating a network similarity matrix (similar to Figure S7 in Gratton et al., 2018). To create the network similarity matrix, we correlated the mean time series within each network in the cortex and cerebellum, separately for split-halves of data. We then created a "second order" similarity matrix by correlating this matrix (upper triangle only for within cerebellum and within cortex comparisons) both within each subject and between each other subject's split have of data. This matrix was then examined for group-level and individual level effects. On-diagonal elements of the network similarity matrix (within-subjects) reflect effects from both the group and individual level. Off-diagonal elements of the matrix (between-subjects) reflect only those effects common across the group (i.e., group level effects) Individual-effects were determined by subtracting the group effect (mean of off-diagonal elements) from the mean of the on-diagonal elements. Differences in group versus individual effects were tested for significance within the cerebellum and cortex – and between the cerebellum and cortex – using paired two-sample t tests.

### Inter-subject RSFC variability

RSFC variance was assessed across the cortex and cerebellum vertex/voxel-wise as the mean standard deviation of Fischer z-transformed correlations from a given vertex/voxel to every other vertex/voxel across subjects. As in previous analyses, we excluded any voxels and vertices within 30mm of the source. Network-level variance in the cortex and cerebellum was calculated as the mean standard deviation across all vertices and voxels, respectively, within a network.

### Functional network variability

We contrasted the variance in the spatial arrangement of networks within each separately. First, we calculated the relative contribution of a given network to the total surface/volume by taking the number of vertices/voxels occupied by a given network in relation to the total number of vertices/voxels,

$$RC_n = 100\ x\ \left(\frac{v_i}{v_e}\right),$$

where $RC_n$ is the relative contribution of a network, $v_i$ is the total volume/area occupied by a network, and $v_e$ is total volume/area. We then calculated the inter-subject variance in relative contribution for each network within the cortex and cerebellum, separately. For each network, the ratio between the two structures was computed and normalized by cortical variance,

$$Var_n = 100\ x\ \left(\frac{var_{cerebellum} + var_{cortex}}{var_{cortex}}\right),$$

where $Var_n$ is the ratio of cerebellar to cortical variance within a network, $var_{cerebellum}$ is the inter-subject variance within a cerebellar network, and $var_{cortex}$ is inter-subject variance within a cortical network. Lastly, global variance was computed by taking the mean across all networks (i.e., the mean of $Var_n$).

To test for a significant difference in the variance in network assignments within the cerebellum versus the cortex ($Var_n$), we generated a null distribution of variance in network assignments by permuting the affiliation of a network to either the cortex or cerebellum 1,000 times and recalculating variance in the relative contribution of a network within both the cerebellum ($var_{cerebellum}$) and cortex ($var_{cortex}$). We then compared the observed variance to the null distribution.

To quantify anatomical variability within a motor system (hand) in the cerebellum, we extracted each subject's convergence patch from the analysis above ('Task/Rest Convergence') and created an overlap of voxels after linear registration of each subject's atlas-transformed cerebellum. To further probe anatomical variability across subjects in peak hand motor representation, we extracted the peak task-evoked BOLD activity in right-hand motor network in the cerebellum (highest Pearson r from the hand motor task). We then correlated the resting state BOLD signal from this peak cerebellar voxel with every hand motor cortical vertex, in each subject. We then calculated the mean correlation and normalized by the number of vertices in the Infomap hand motor patch, within a given individual and across all MSC subjects. This process was repeated for each subject, resulting in a subject x subject matrix of correlation values. Diagonal elements represent the 'matching' correlation (e.g., correlation between hand motor cerebellum and hand motor cortex in MSC 02), whereas off-diagonal elements represent 'mismatching' correlations (e.g., correlation between hand motor cerebellum in MSC 02 and hand motor cortex in MSC 06). We determined the magnitude of subject variability in hand motor representation in the cerebellum by calculating the mean and standard deviation of Euclidean distance between peak cerebellar coordinates across subjects.

### Relative network proportions in the cerebellum versus cortex

For each network, the fraction of the cortex and cerebellum occupying the total surface/volume was calculated within each subject as in the variance analysis in network assignments above for the cortical surface and cerebellum separately. The between subject average for each network was then calculated. We then plotted the mean network representation in the cerebellum against the mean network representation in the cortex. The relative proportion occupied by a given network in the cerebellum versus the cortex was calculated as a ratio of the two:

$$R_n = \frac{Cereb_n}{Cort_n},$$

where $R_n$ is the ratio of a network's representation in the cerebellum ($Cereb_n$) versus the cortex ($Cort_n$). Values near one indicate equal representation in the cerebellum as in the cortex. Values greater than one indicate greater representation in the cerebellum, whereas values less than one indicate greater relative representation of a network in the cortex.

### Cerebellar Lead/Lag Analysis

We used a previously published method for computing time delay estimates as described in detail elsewhere (Mitra et al., 2014, 2015). Briefly, for each session, we first computed a lagged cross-covariance function (CCF) between each pair of vertices/voxels at a temporal resolution of the acquired data (volume TR = 2200ms). To account for censored frames, we computed CCFs over blocks of contiguous frames and averaged these CCFs, weighted by block duration, to obtain a single CCF for the session. We excluded time delays greater than 4 s as, in our experience, these tend to reflect sampling error or artifact. Thus, CCFs were only computed over three TR shifts in the positive and negative directions, making the minimum block duration [3 (TR shifts) + 1 (zero-lag)]*TR = 8.8 s. Lags were then more precisely determined by estimating the cross-covariance extremum of the session-level CCF using three-point parabolic interpolation. The resulting set of lags was assembled into an antisymmetric matrix capturing all possible pairwise time delays (TD matrix) for each session, which was averaged across sessions and subjects to yield subject- and group-level TD matrices, respectively. The TD matrix was sorted from early to late, by resting state network, and finally, by brain structure (i.e., cortex versus cerebellum), to aid in visualization of propagation within and between networks (Mitra et al., 2014) and brain structures.

We additionally computed ''lag projection'' maps (Mitra et al., 2014) for the cerebellum based exclusively on its relationship with cortex. Thus, for each cerebellar voxel we computed its mean latency across all cortical vertices. The resulting lag projection map of the cerebellum reflects the average latency of each cerebellar voxel with respect to the cortex, with positive values reflecting late activity in the cerebellum relative to the cortex.

### Non-linear registration of volumetric time series

Differences in inter-subject variance of RSFC and network organization within the cerebellum and between the cerebellum and cortex may be explained, in part, by the differential handling of these two structures (i.e., surface data within the cortex, volumetric data within the cerebellum). For each subject, the atlas-transformed T1-weighted image was non-linearly registered to a reference subject (MSC 01) using FSL's FNIRT. Subsequently, volumetric time series files were non-linearly registered to each subject's registered T1-weighted image. Session-level time series were concatenated and temporally masked for high motion frames (FD > 0.2 or DVARS > 5.36). Cortical voxels within 30mm (Euclidean distance) of a cerebellar voxel were not included in subsequent analyses.

We then recomputed the following: (i) split-half RSFC reliability across the cerebellum and cortex, (ii) standard deviation of RSFC across subjects in the cortex and cerebellum, (iii) network organization using Infomap (see below), (iv) RSFC similarity, (v) frontoparietal network representation in the cortex and cerebellum. For our voxel-wise parcellation using Infomap, we thresholded (0.5% and 1%) the full adjacency matrix (cortex plus cerebellum) in a structure-specific manner, such that each structure (cortex and cerebellum) – in addition to the links between cortex and cerebellum – were equal in number.

## DATA AND SOFTWARE AVAILABILITY

Raw MRI data, as well as segmented cortical surfaces, preprocessed volumetric and cifti-space RSFC time courses, myelin maps, and individual-specific parcellations and networks, will be deposited in the Openfmri data repository (https://openfmri.org/) under the label "Midnight Scan Club." Session- and subject-specific volumetric task responses will be deposited in the Neurovault repository (https://neurovault.org/) under the label "Midnight Scan Club task data."

Neuron, Volume *100*

## Supplemental Information

# Spatial and Temporal Organization of the Individual Human Cerebellum

**Scott Marek, Joshua S. Siegel, Evan M. Gordon, Ryan V. Raut, Caterina Gratton, Dillan J. Newbold, Mario Ortega, Timothy O. Laumann, Babatunde Adeyemo, Derek B. Miller, Annie Zheng, Katherine C. Lopez, Jeffrey J. Berg, Rebecca S. Coalson, Annie L. Nguyen, Donna Dierker, Andrew N. Van, Catherine R. Hoyt, Kathleen B. McDermott, Scott A. Norris, Joshua S. Shimony, Abraham Z. Snyder, Steven M. Nelson, Deanna M. Barch, Bradley L. Schlaggar, Marcus E. Raichle, Steven E. Petersen, Deanna J. Greene, and Nico U.F. Dosenbach**

# SUPPLEMENTARY MATERIAL

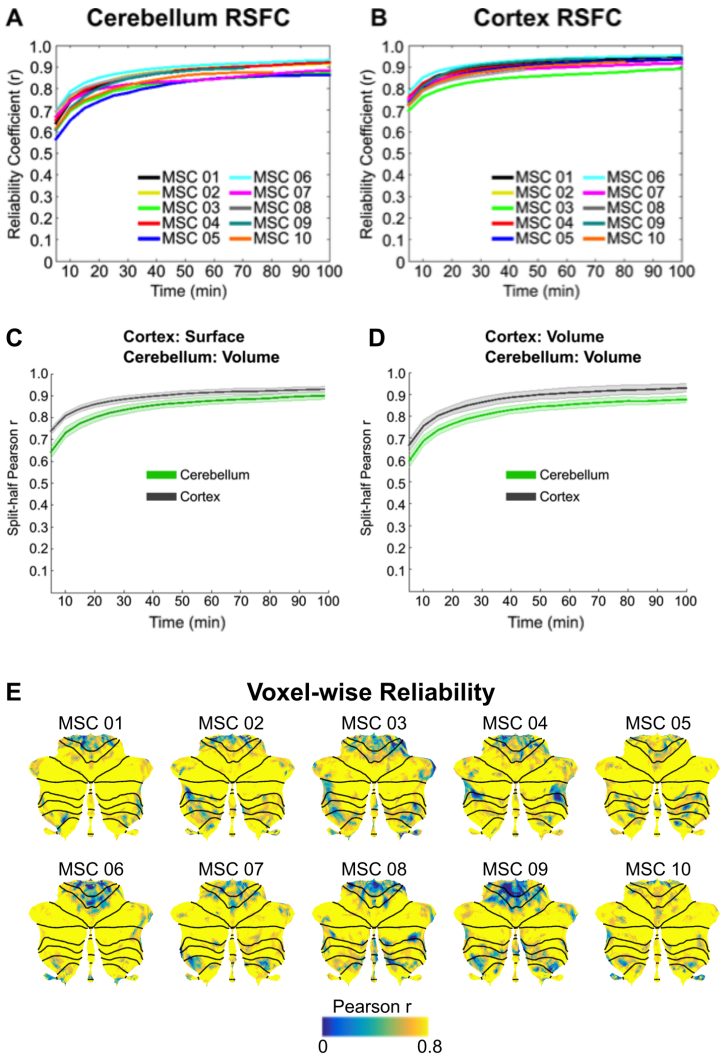


**Figure S1. Reliable cerebellar RSFC estimation requires large quantities of data, Related to Figure 1.** The split-half reliability of individual subject RSFC in the **(A)** cerebellum and **(B)** cortex increase with larger quantities of data. A given quantity of post motion-censored data (test set) was randomly selected and compared to an independent comparison set of data from the same subject, repeated 1,000 times for each time interval. **(C)** Average reliability across subjects for the cerebellum (voxels) and cortex (vertices), demonstrating relatively larger quantities of RSFC data are needed in the cerebellum to achieve similar reliability to the cortex. **(D)** Average reliability across subjects for the cerebellum (voxels) and cortex (voxels). Note the similarity in panels **C** and **D**, supporting the notion that reliability does not change if vertices vs. voxels are used to measure the cortex. Shaded bars in **C** and **D** denote standard error of the mean across subjects. **(E)** Voxel-wise split-half reliability of cerebellar RSFC represented on a flat map.

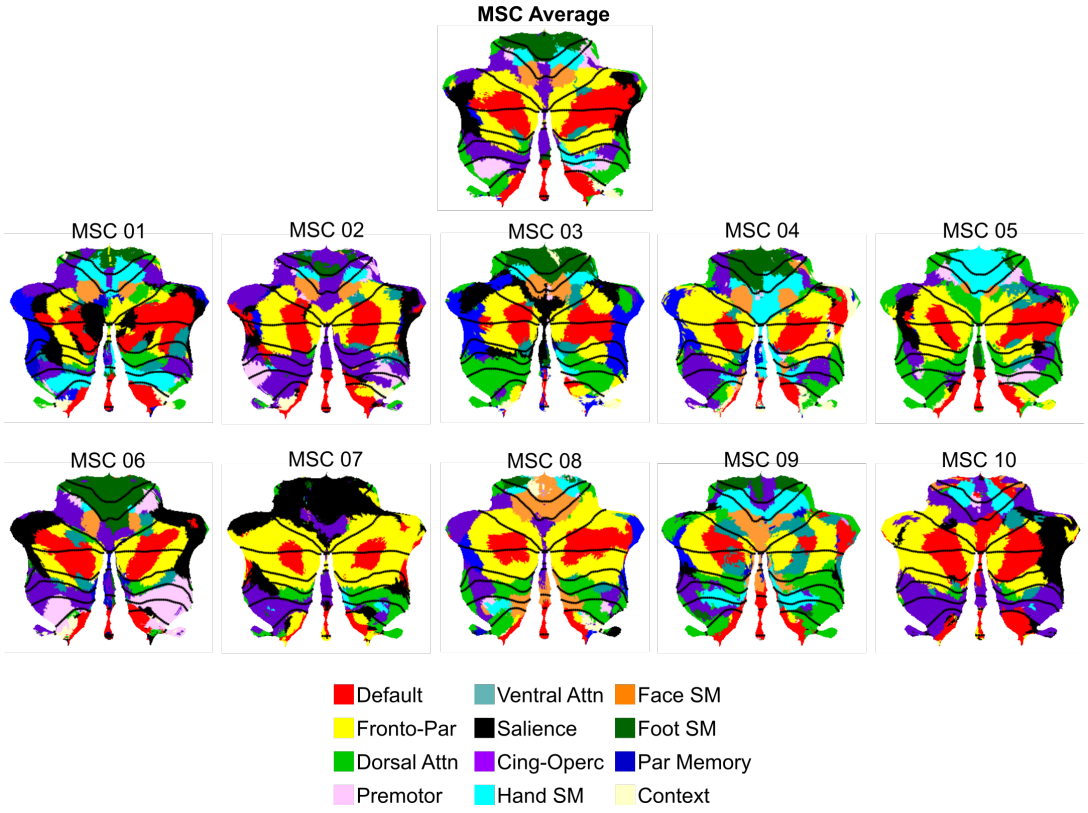


**Figure S2. Flat map representations of winner-take-all assignments in the MSC average and individual subjects, Related to Figure 1.** MSC average and individual MSC winner-take-all network partitions. Qualitatively, considerable variance exists between MSC subjects and between each subject and the group average. Anatomical coordinates are the same for each MSC subject as in the MSC Average.

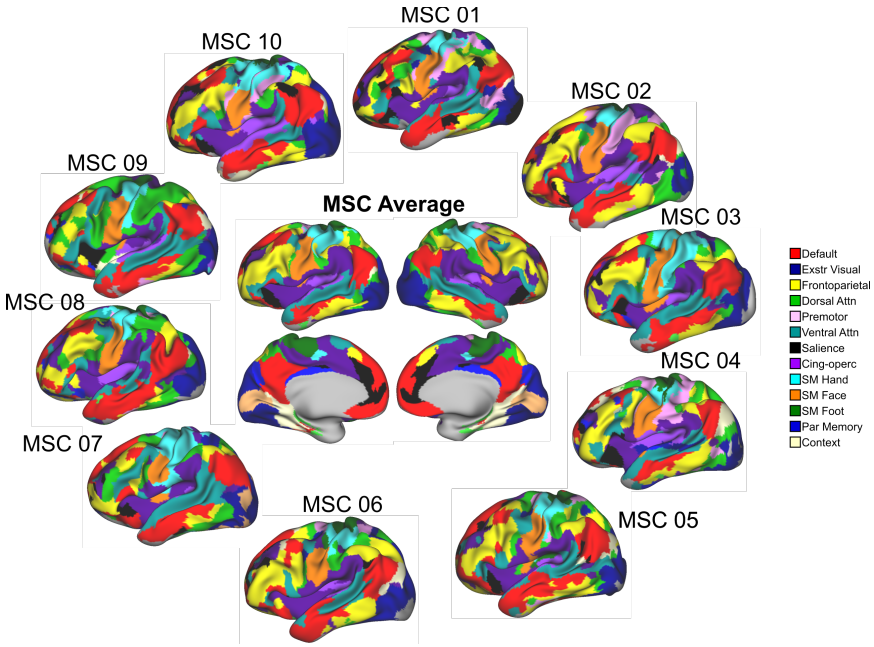


**Figure S3. Cortical resting state networks from highly-sampled MSC subjects, Related to Figure 1.** Outer ring: Left lateral view of individual functional brain networks. Middle panel: MSC average left and right (lateral and medial) view of functional brain networks. Individuals demonstrate measurable network pieces that deviate from the group average.

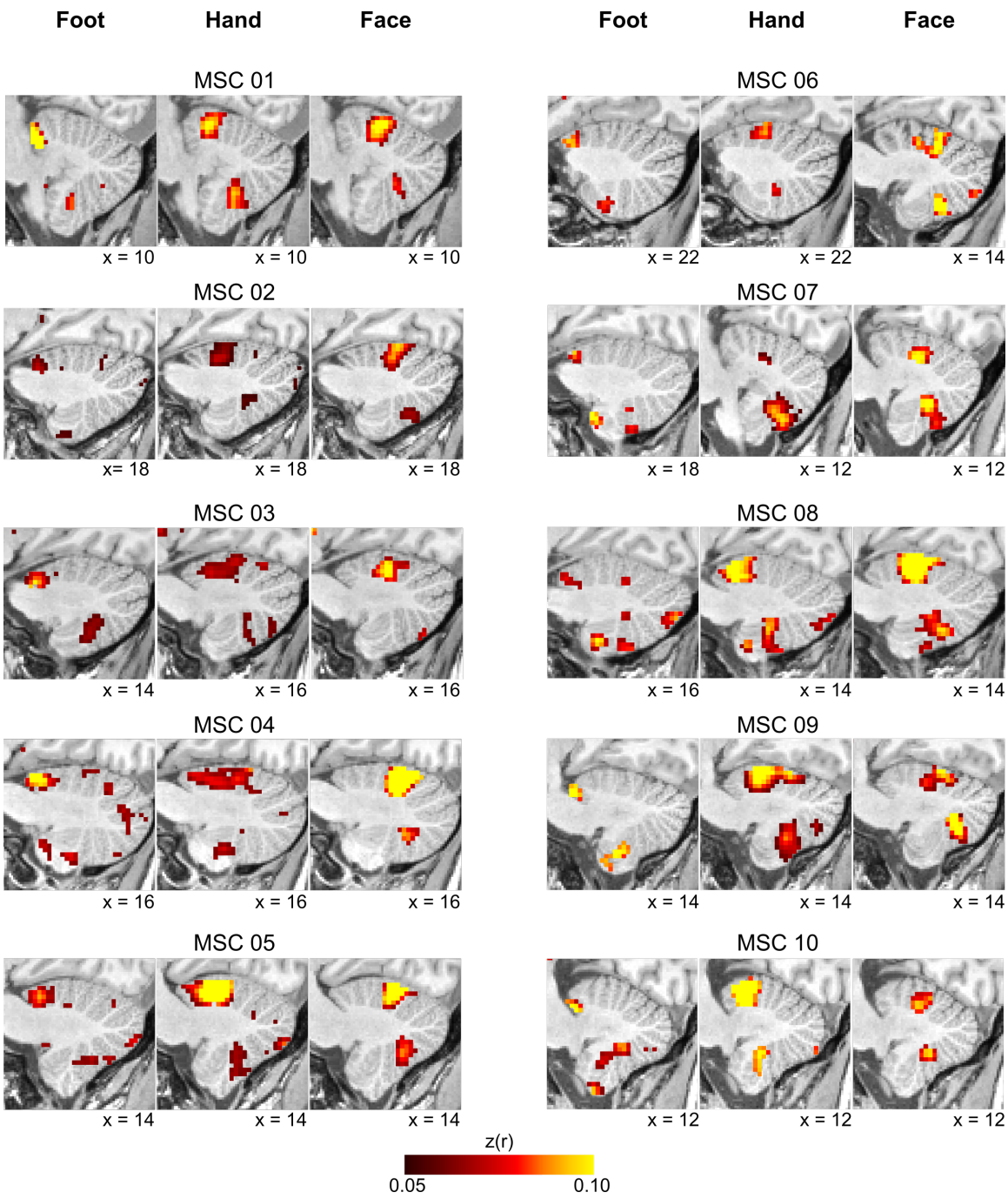


**Figure S4. Cerebellar seed maps of primary motor networks, Related to Figures 2 and 3.** For each subject and each motor network (foot, hand, face), we created seeded correlations from the cortical vertex demonstrating the greatest task-evoked response to all cerebellar voxels. Within each subject, we observed both an anterior and posterior representation of each motor network, providing further evidence that the quality of our individual subject data was sufficient to realize the expected double representation of the cerebellar motor homunculus.

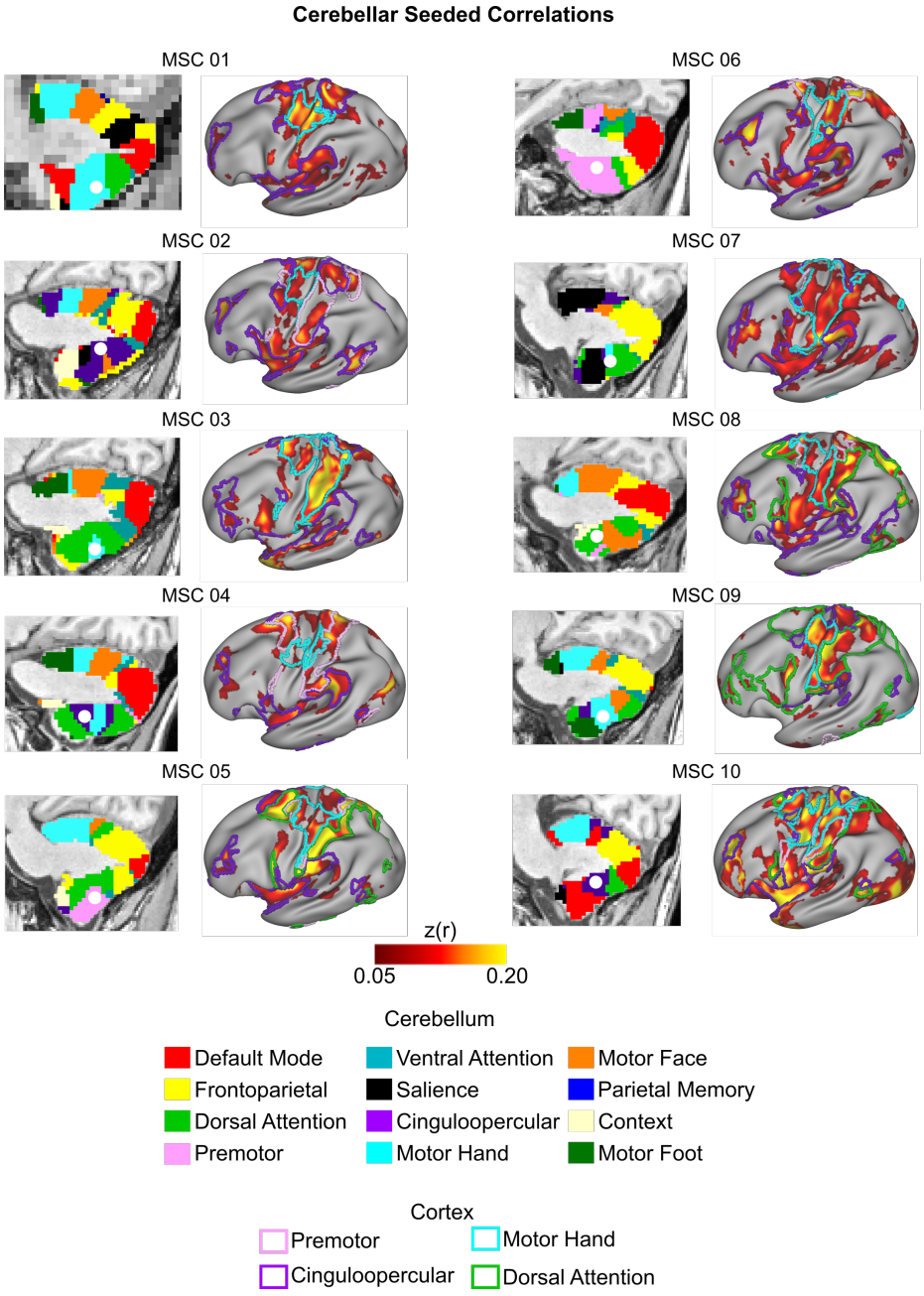


**Figure S5. Cortical RSFC maps from posterior cerebellum seeds, Related to Figures 2 and 3.** For each subject, we chose a seed from the posterior motor hand representation (middle column in Figure 7 within this document) and displayed RSFC between this voxel and each cortical vertex. The cortical network boundaries are displayed in colored outline on the cortical surface. Generally, these posterior seeds were highly correlated with premotor and cinguloopercular networks, in addition to the motor hand network. This raises the possibility that posterior regions of the cerebellum may play integrative role in motor control.

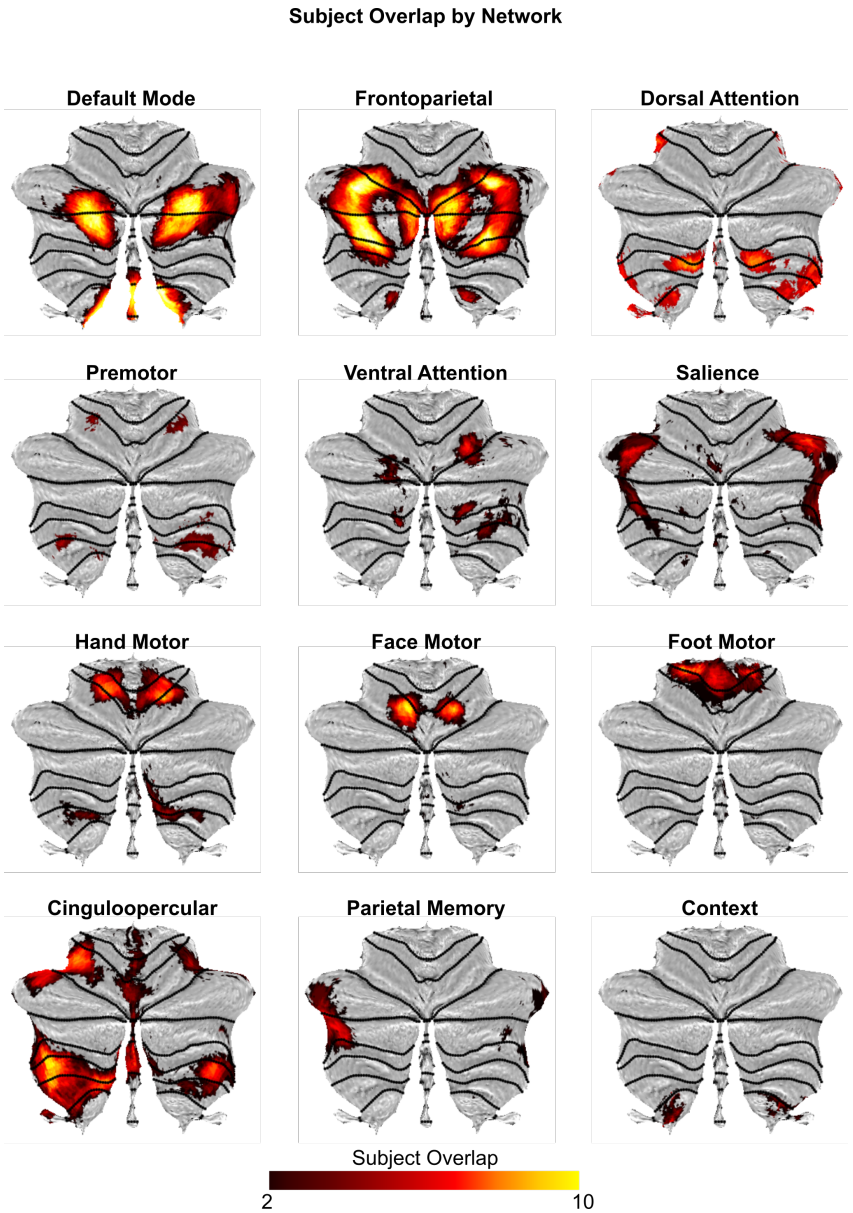


**Figure S6. Subject overlap in winner-take-all assignments, zrelated to Figure 5B**. For each network across the cerebellum, we quantified the number of subjects with a given network assignment. The magnitude of overlap is represented in color, where darker shades of red indicate relatively little subject overlap and yellow shades indicates relatively greater subject overlap.

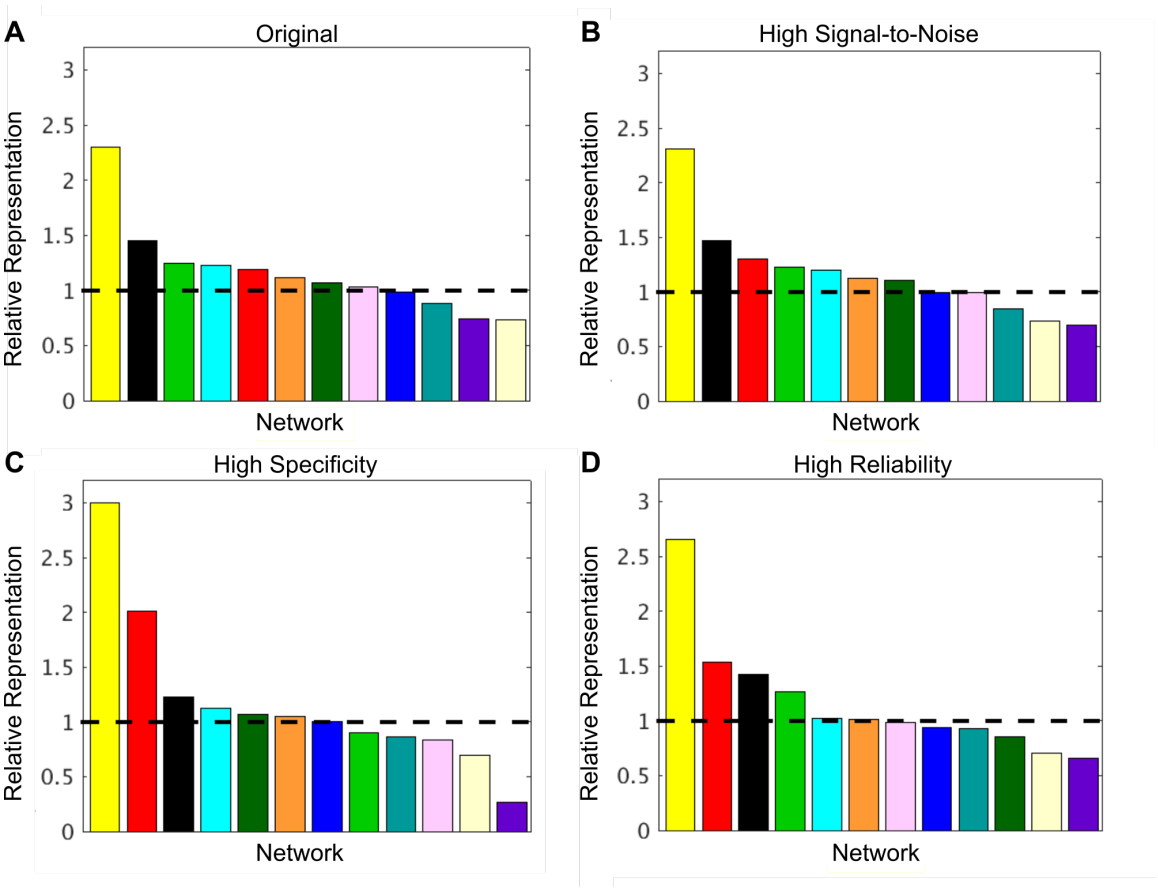


**Figure S7. Frontoparietal overrepresentation estimation is robust to voxels with low tSNR, low specificity, and low split-half reliability, Related to Figure 6**. **(A)** Original estimates of relative ratio (cerebellum/cortex) of network representation as in Figure 6D. Subsequent figures of the relative ratio of network representations after only including cerebellar voxels with **(B)** high tSNR (>2.5), **(C)** high specificity (>50%), and **(D)** high reliability (> 0.70). Values greater than one (horizontal dotted line) indicate greater relative space occupied by a network in the cerebellum, whereas values less than one indicate greater space occupied by a network in the cortex. In each case, the estimate of frontoparietal overrepresentation in the cerebellum compared to cortex is greater than or equal to 2.3-fold as reported in the main text.

**Table S1. Difference in posterior and anterior cerebellum lags (ms) by network, Related to Figure 7.**

| | DMN | FPN | DAN | PM | VAN | SAL | CON | Hand | Face | ParM | CTX | Foot |
|---|---|---|---|---|---|---|---|---|---|---|---|---|
| MSC 01 | -19.2 | 177.5 | 42.1 | - | 34.9 | 103.0 | -26.2 | 122.4 | - | 78.2 | 20.3 | 178.2 |
| MSC 02 | 1.3 | 77.9 | -29.3 | -10.2 | 74.9 | 53.3 | 15.6 | -31.0 | -85.0 | -1.7 | -54.2 | 73.4 |
| MSC 03 | -134.9 | -15.0 | -84.5 | -49.2 | -106.1 | 50.7 | -217.7 | -128.7 | - | 83.6 | 49.7 | -117.2 |
| MSC 04 | -108.1 | -45.4 | -121.9 | -52.5 | -75.6 | -236.7 | -150.4 | -113.5 | -100.1 | -203.7 | -56.8 | -23.2 |
| MSC 05 | -170.7 | -25.2 | -35.0 | -3.5 | -156.3 | -162.2 | -81.2 | - | - | -119.3 | - | 46.1 |
| MSC 06 | -89.7 | -18.5 | -19.4 | -6.0 | -49.6 | -18.2 | 27.1 | - | - | - | -12.2 | 54.7 |
| MSC 07 | -162.9 | 31.0 | -21.9 | - | -61.4 | -36.7 | -79.7 | 18.0 | -88.3 | - | - | 139.3 |
| MSC 08 | -121.5 | 4.1 | 31.4 | 25.2 | -39.5 | -5.0 | 122.2 | 37.3 | 89.7 | 100.5 | 136.9 | 85.0 |
| MSC 09 | -144.0 | -23.9 | 49.6 | -72.7 | 19.7 | 109.6 | 120.8 | 46.5 | 25.4 | 118.5 | -80.2 | 3.3 |
| MSC 10 | -52.2 | 74.6 | 186.9 | 152.6 | 47.1 | 125.9 | -49.5 | -4.3 | - | - | - | - |
| **Avg** | **-100.2** | **23.7** | **-0.2** | **-2.0** | **-31.2** | **-1.6** | **-31.9** | **-6.7** | **-31.6** | **8.0** | **0.5** | **48.9** |

*Sign = posterior – anterior;
- Indicates no winner take all representation in either an anterior or posterior representation.
DMN = default mode network; FPN = frontoparietal network; DAN = dorsal attention network; PM = premotor network; VAN = ventral attention network; SAL = salience network; CON = cingulo-opercular network; Hand =hand motor network; Face = face motor network; ParM = parietal memory network; CTX = context network; Foot = foot motor network.